Calculation of Zero-Field Splittings, g-Values, and the Relativistic Nephelauxetic Effect in Transition Metal Complexes. Application to High-Spin Ferric Complexes†

Frank Neese and Edward I. Solomon*

Department of Chemistry, Stanford University, Stanford, California 94305

Received August 11, 1998

Equations are derived and discussed that allow the computation of zero-field splitting (ZFS) tensors in transition metal complexes for any value of the ground-state total spin *S*. An effective Hamiltonian technique is used and the calculation is carried to second order for orbitally nondegenerate ground states. The theory includes contributions from excited states of spin S and $S \pm 1$. This makes the theory more general than earlier treatments. Explicit equations are derived for the case where all states are well described by single-determinantal wave functions, for example restricted open shell Hartree−Fock (HF) and spin-polarized HF or density functional (DFT) calculation schemes. Matrix elements are evaluated for many electron wave functions that result from a molecular orbital (MO) treatment including configuration interaction (CI). A computational implementation in terms of bonded functions is outlined. The problem of ZFS in high-spin ferric complexes is treated at some length, and contributions due to low-symmetry distortions, anisotropic covalency, charge-transfer states, and ligand spin−orbit coupling are discussed. ROHF-INDO/S-CI results are presented for $FeCl_4^-$ and used to evaluate the importance of the various terms. Finally, contributions to the experimentally observed reduction of the metal spin−orbit coupling constants (the relativistic nephelauxetic effect) are discussed. B3LYP and Hartree−Fock calculations for $FeCl_4^-$ are used to characterize the change of the iron 3d radial function upon complex formation. It is found that the iron 3d radial distribution function is significantly expanded and that the expansion is anisotropic. This is interpreted as a combination of reduction in effective charge on the metal 3d electrons (central field covalence) together with expansive promotion effects that are a necessary consequence of chemical bond formation. The $\langle \mathbf{r}^{-3} \rangle_{3d}$ values that are important in the interpretation of magnetic data are up to 15% reduced from their free-ion value before any metal−ligand orbital mixing (symmetry-restricted covalency) is taken into account. Thus the use of free-ion values for spin−orbit coupling and related constants in the analysis of experimental data leads to values for MO coefficients that overestimate the metal−ligand covalency.

1. Introduction

Transition metal complexes play important roles as catalysts in the active sites of metalloenzymes and in industrial processes.[1] In many cases high-resolution crystal structures for the sites are not available, and spectroscopic studies are relied upon to provide structural information. This is especially important for the study of reaction intermediates. Complementary to crystallography, spectroscopic techniques provide information about the electronic structures of the sites which are intimately linked to their reactivities.[2] To maximize the amount of information obtained from spectroscopic studies, theoretical models are required that connect the active site geometric and electronic structure to the observed spectra.

Since transition metal complexes are frequently paramagnetic, a great deal of information is obtainable from magnetic spectroscopies such as EPR, ENDOR, ESEEM, MCD, ODMR, and Mössbauer spectroscopy.[3] All of these methods are sensitive to the magnetic properties of the electronic-ground state configuration. Traditionally, the splittings of the ground configuration sublevels are described by a spin Hamiltonian (SH) which introduces an effective spin *S* of the state under consideration and absorbs the spatial degrees of freedom into a small set of numerical parameters.[4,5] In this way the data analysis is divided into two steps: fitting SH parameters to experimental spectra and their interpretation using an appropriate theoretical method. The second step is frequently not carried out, and many empirical relations for the SH parameters have been used to great advantage by experimentalists (i.e., ref. 6). However, this step is required if the goal of the investigation is a detailed

* Author to whom correspondence should be addressed.

† Abbreviations used: INDO/S, intermediate neglect of differential overlap/spectroscopic parametrization; CI, configuration interaction; ROHF, restricted open shell Hartree Fock; EPR, electron paramagnetic resonance; ENDOR, electron nuclear double resonance; ESEEM, electron spin echo envelope modulation; MCD, magnetic circular dichroism; ODMR, optically detected magnetic resonance; B3LYP, Becke three parameter hybrid density functional with Lee−Yang−Parr correlation part.

(1) Holm, R. H.; Kennepohl, P.; Solomon, E. I. *Chem. Rev.* **1996**, *96*, 2239, and other articles in the same volume.
(2) Solomon, E. I.; Lowery, M. D. *Science* **1993**, *259*, 1575.
(3) (a) Solomon, E. I. *Comments Inorg. Chem.* **1984**, *3*, 227. (b) Solomon, E. I.; Hanson, M. A. In *Inorganic Electronic Spectroscopy*; Solomon, E. I., Lever, A. B. P., Eds.; Wiley & Sons: New York, in press.
(4) Abragam, A.; Bleaney, B. *Electron Paramagnetic Resonance of Transition Ions*; Clarendon Press: Oxford, 1970.
(5) (a) Pake G. E.; Estle T. L. *The Physical Principles of Electron Paramagnetic Resonance*; W. A. Benjamin Inc.: London, 1973. (b) Carrington, A.; McLachlan A. D. *Introduction to Magnetic Resonance*; Wiley Interscience: New York, Evanston, London, 1967. (c) Atherton, N. M. *Principles of Electron Spin Resonance*, 2nd ed.; Ellis Horwood, Prentice-Hall: New York, 1993. (d) Slichter, C. P. *Principles of Magnetic Resonance, 3rd ed.*; Springer Series in Solid State Sciences 1; Springer: Berlin, 1990. (e) Pilbrow, J. R. *Transition Ion Electron Paramagnetic Resonance*; Clarendon Press: Oxford, 1990.
(6) (a) Blumberg, W. E.; Peisach, J. In *Probes of Structure and Function of Macromolecules and Membranes*; Chance, B., Yonetani, T., Mildva, A. S., Eds.; Academic Press: New York, 1971; Vol. 2, pp 215ff. (b) Peisach, J.; Blumberg, W. E. *Arch. Biochem. Biophys.* **1974**, *165*, 691.

10.1021/ic980948i CCC: $15.00
Published on Web 12/03/1998

electronic structure description of the compound under investigation and is the focus of this paper.

The SH was first introduced by Abragam and Pryce[7] in the context of crystal field theory (CFT) and elaborated by others.[8] In analyzing experimental results, it has generally been found that spin−orbit coupling (SOC) constants that are reduced from the value of the free ion are required, and this has been called the relativistic nephelauxetic effect[9] because the spin−orbit coupling effect is relativistic in origin and the reduction could be explained by an expansion of the metal−radial probability distribution function.[9] Detailed accounts of these developments are available[10,11] and are still used in the ligand field theory and angular overlap approaches.[12]

On the basis of the nephelauxetic effect and the observation of ligand hyperfine interactions,[13] it became clear that metal−ligand covalency should be accounted for in more detail, and molecular orbital (MO) models were developed for *g*-values, hyperfine couplings,[14] and ZFSs.[14d,15] Importantly, the combined experimental and theoretical study of the ZFS in high-spin ferric complexes[16−18] showed that Griffith's model[19] predicts the wrong sign for the ZFS in the case of $FeCl_4^-$ and that this can be traced back to the differential convalencies of the predominantly Fe-3d MOs, thus underlining the importance of an explicit consideration of covalency.

The question arises of how the spin Hamiltonian parameters can be calculated in the general case where no specific approximation (MO, valence bond, ligand field, etc.) to the nonrelativistic many-electron wave functions is assumed. This problem has been analyzed by several authors,[20−22] but applications of these theories to transition metal complexes are scarce. McWeeny has developed a transparent approach to the calculation of *g*-values and ZFSs.[20] However, his results only include the case where spin−orbit coupling occurs between states of the same spin.[20] This restriction is unsatisfactory for many applications and especially for the ZFSs of high-spin ferric complexes where the SOC between the ground sextet and low lying excited state quartet states makes a major contribution to the ZFS.[16−19]

Therefore an extension of McWeeny's treatment is necessary and is developed in sections 2.1−2.4 of this paper. Readers not interested in the derivation can proceed directly to the results in eqs 16, 18, 30, and 31. In sections 2.5 and 2.6 the numerical implementation in terms of MO and CI wave functions is presented. On the basis of these developments, the ZFSs of high-spin ferric complexes are analyzed in section 3 and contributions due to low-symmetry ligand field splittings, anisotropic covalency, charge-transfer states, and ligand spin−orbit coupling are identified (section 3.1). The various contributions are then evaluated through INDO/S-CI calculations for the specific case of $FeCl_4^-$ (section 3.2). This complex was chosen as a representative for high-spin ferric systems with axial ZFS, because (1) it is a relatively simple, high-symmetry system, (2) it has been intensely studied at the single-crystal level with ground- and excited-state spectroscopies and the second- and fourth-order contributions to the observed ZFS have been experimentally determined,[16,17] and (3) the origin of the ZFS in this complex has been analyzed in detail.[16,17]

It is commonly assumed that the free-ion SOC constants obtained from atomic spectroscopy are suitable to calculate **g**-matrices and **D**-tensors. However, these constants depend on the radial distribution function of the metal and ligand orbitals involved in bonding, and the changes of these radial functions upon complex formation have received little attention. Therefore section 4 of the paper evaluates the changes in the metal 3d radial distribution functions for the special case of $FeCl_4^-$ using the Hartree−Fock and B3LYP electronic structure methods. Finally, the connection to ligand-field models is developed (section 4.3), and the contributions to the total reduction in the apparent metal spin−orbit coupling are discussed (section 4.4).

2. Theory

In the absence of nuclear spins and exchange interactions, the spin Hamiltonian up to terms bilinear in the effective spin is usually written[4]

$$H_{spin} = H_{Ze} + H_{ZFS} = \beta_B \vec{B}\mathbf{g}\vec{S} + \vec{S}\mathbf{D}\vec{S} \quad (1)$$

where β_B is the Bohr magneton, $\vec{B}$ is the magnetic flux density, $\vec{S}$ is the operator for the effective spin, and **g** and **D** are the **g**-matrix and the ZFS-tensor, respectively. H_{spin} acts on the basis functions $|SM\rangle$ with $M = S, S-1, ..., -S$. If a coordinate system is chosen that diagonalizes **D**, H_{ZFS} can be rewritten:

$$H_{ZFS} = D[S_z^2 - {}^1/_3 S(S+1)] + E[S_x^2 - S_y^2] \quad (2)$$

$$D = D_{zz} - {}^1/_2(D_{xx} + D_{yy}); \quad E = {}^1/_2(D_{xx} - D_{yy}) \quad (3)$$

A constant ${}^1/_3(D_{xx} + D_{yy} + D_{zz})S(S+1)$ is dropped because it shifts all levels equally, and the factor $-{}^1/_3 DS(S+1)$ is introduced for convenience. In a proper coordinate system *x*, *y*, and *z* are chosen such that $0 \le E/D \le {}^1/_3$.[23,24] Note that in

(7) (a) Pryce, M. H. L. *Proc. Phys. Soc. (London)* **1950**, *A63*, 25. (b) Abragam, A.; Pryce, M. H. L. *Proc. R. Soc.* **1951**, *A205*, 135.
(8) (a) Bleaney, B.; Stevens, K. H. W. *Rep. Prog. Phys.* **1953**, *16*, 108. (b) Stevens, K. H. W. In *Magnetism*; Rado, G. T., Suhl, H., Eds.; Academic Press: New York, 1963, pp 1ff. (c) Griffith, J. S. *Mol. Phys.* **1959**, *3*, 79.
(9) (a) Jørgensen, C. K. *Orbitals in Atoms and Molecules*; Academic Press: London, 1962. (b) Jørgensen, C. K. *Adv. Chem. Phys.* **1963**, *V*, 33. (c) Jørgensen, C. K. *Struc. Bond.* **1969**, *6*, 94. (d) Jørgensen, C. K. *Struc. Bond.* **1966**, *1*, 3. See also: (e) Belford, R. L.; Karplus, M. *J. Chem. Phys.* **1959**, *31*, 394.
(10) Griffith, J. S. *The Theory of Transition Metal Ions*; Cambridge University Press: Cambridge, 1964.
(11) Ballhausen, C. J. *Introduction to Ligand Field Theory*; McGraw Hill Inc.: New York, 1962.
(12) Bencini, A.; Benelli, C.; Gateschi, D. *Coord. Chem. Rev.* **1984**, *60*, 131.
(13) Griffith, J. H. E.; Owen, J. *Proc. R. Soc. (London)* **1954**, *A226*, 96.
(14) (a) Stone, A. J. *Proc. R. Soc. (London)* **1963**, *A271*, 424. (b) Maki, A. H.; McGarvey, B. R. *J. Chem. Phys.* **1958**, *29*, 31; *Ibid*. 34. (c) Kivelson, D.; Neimann, R. *J. Chem. Phys.* **1961**, *35*, 149. (d) McGarvey, B. R. *Transition Metal Chem.* **1966**, *3*, 89. (e) Keijzers, C. P.; DeBoer, E. *J. Chem. Phys.* **1972**, *57*, 1277. (f) Smith, D. W. *J. Chem. Soc. A* **1970**, 3108.
(15) McGarvey, B. R. *J. Chem. Phys.* **1964**, *41*, 3743.
(16) Gebhard, M. S.; Deaton, J. C.; Koch, S. A.; Millar, M.; Solomon, E. I. *J. Am. Chem. Soc.* **1990**, *112*, 2217.
(17) Deaton, J. C.; Gebhard, M. S.; Solomon, E. I. *Inorg. Chem.* **1989**, *28*, 877.
(18) Zhang, Y.; Gebhard, M. S.; Solomon, E. I. *J. Am. Chem. Soc.* **1991**, *117*, 7422.
(19) Griffith, J. S. *Mol. Phys.* **1964**, *8*, 213.
(20) (a) McWeeny, R. *Methods of Molecular Quantum Mechanics*; Academic Press: London, 1992. (b) McWeeny, R. *Spins in Chemistry*; Academic Press: New York, 1970. (c) McWeeny, R. *J. Chem. Phys.* **1965**, *42*, 1717.
(21) Atkins, P. W.; Jamieson, A. M. *Mol. Phys.* **1967**, *14*, 425.
(22) Harriman, J. E. *Theoretical Foundations of Electron Spin Resonance*; Academic Press: New York, 1978.
(23) Blumberg, W. E. In *Magnetic Resonance in Biological Systems*; Ehrenberg, A., Malmström, B., Eds.; Pergamon Press: Oxford, 1967; pp 110ff.
(24) Gaffney, B. J.; Silverstone, H. J. In *EMR of Paramagnetic Molecules*; Berliner, L. J., Reuben, J., Eds.; Plenum Press: New York, 1993; pp 1ff.

general $D_{xx} + D_{yy} + D_{zz} \neq 0$; the **D**-tensor is not in general traceless, as is sometimes stated.

2.1. Origin of Spin Hamiltonian Parameters. To connect **g** and **D** with exact or approximate eigenfunctions of the Born−Oppenheimer (BO) Hamiltonian, an effective Hamiltonian technique is used.[20,25] An orthonormal set of many-electron wave functions $\{|\alpha S_\alpha M\rangle\}$ is assumed, where α is a compound label that contains all necessary quantum numbers except S_α and M, the total spin of state α, and its projection onto the z-axis ($M = S_\alpha, S_\alpha - 1, ..., -S_\alpha$). The set of states is assumed to diagonalize the BO Hamiltonian, i.e., $H_{BO}|\alpha S_\alpha M\rangle = E_\alpha|\alpha S_\alpha M\rangle$, and states are labeled in order of increasing energy. Since H_{BO} commutes with the S^2 operator, S_α and M are good quantum numbers. The full Hamiltonian is taken to be

$$H = H_{BO} + H_1 \tag{4}$$

where $H_1 = H_{SOC} + H_{ZE}$. H_{ZE} is the Zeeman operator; H_{SOC} the SOC operator (see below). In the effective Hamiltonian approach, the set of states is divided into *a*- and *b*-sets. In the present treatment it is required that the ground state is only spin-degenerate; that is, the *a*-set contains $2S_a + 1$ functions $|aS_aM\rangle$, while the *b*-set contains all other functions. The goal is to absorb the effect of the *b*-set on the *a*-set states into a small set of numerical parameters so that the matrix of the effective Hamiltonian, H_{eff}, in the basis of the perturbed *a*-set functions can be identified with the matrix of the spin Hamiltonian. Following McWeeny,[20] one obtains for the matrix elements of the effective Hamiltonian

$$\langle aS_aM|H_{eff}|aS_aM'\rangle = E_a\delta_{MM'} + \langle aS_aM|H_1|aS_aM'\rangle - \sum_{bM''}\Delta_b^{-1}\langle aS_aM|H_1|bS_bM''\rangle\langle bS_bM''|H_1|aS_aM'\rangle \tag{5}$$

where $\Delta_b = E_b - E_a$, a positive quantity, and E_a is conveniently set to zero. The connection to the spin Hamiltonian formalism is made by requiring that the matrix elements $\langle aS_aM|H_{eff}|aS_aM'\rangle$ are equal to $\langle SM|H_{spin}|SM'\rangle$. With the present choice of H_1, the first-order contribution to the **g**-matrix is a diagonal matrix with elements g_e, the free electron g-value, while there is no contribution to the **D**-tensor. It is well-known that the direct spin−spin dipolar interaction gives a traceless first-order contribution to the **D**-tensor.[20,26] For transition metal complexes it is usually assumed that the second-order contribution to the **D**-tensor, which originates from SOC, is dominant,[5,14d] and this is the focus of the present paper. The **g**-matrix will be written $\mathbf{g} = g_e\mathbf{1} + \Delta\mathbf{g}$, where **1** is a 3×3 unit matrix.

2.2. Spin−Orbit Coupling. The SOC operator in the Breit−Pauli approximation is composed of one- and two-electron contributions and is relatively difficult to handle even in the case of atoms.[27] The usual approach for molecules is to approximate H_{SOC} by an effective one-electron operator of the form[28]

$$H'_{SOC} = \sum_i\sum_A \xi(r_{iA})\vec{l}_A(i)\,\vec{s}(i) = \sum_m (-1)^m \sum_i h_{-m}(i)\,s_m(i) \tag{6}$$

where A sums over all nuclei, $\vec{l}_A(i)$ is the angular momentum of electron i relative to atom A, $\vec{s}(i)$ is the spin operator for the ith electron, and $\xi(r_{iA})$ is a radial operator that is proportional to the inverse third power of the distance of electron i to nucleus A ($r_{iA} = |\vec{r}_i - \vec{R}_A|$; $\vec{R}_A$ is the position of the Ath nucleus). In atomic units[29]

$$\xi(|\vec{r}_i - \vec{R}_A|) = \frac{\alpha^2}{2}\frac{Z_{eff}^A}{|\vec{r}_i - \vec{R}_A|^3} \tag{7}$$

where α is the fine structure constant ($\approx 1/137$), s_m is a standard component of the spin vector operator ($m = -1, 0, 1$), and h_{-m} is a standard component of a reduced spin−orbit vector operator. Note that this form of H'_{SOC} assumes a spherically symmetric electric field around each nucleus.

Since $\vec{s}(i)$ is of type T^{10} with respect to the total spin $\vec{S} = \sum_i\vec{s}(i)$, one can apply the Wigner−Eckhard theorem to each operator of the form $\sum_i f(i)\,s_m(i)$:[20]

$$\langle aS_aM|\sum_i f(i)\,s_m(i)|bS_bM'\rangle = \begin{pmatrix} S_b & 1 & S_a \\ M' & m & M \end{pmatrix}\langle aS_a||\sum_i f(i)||bS_b\rangle \tag{8}$$

where

$$\begin{pmatrix} S_b & 1 & S_a \\ M' & m & M \end{pmatrix}$$

is a Clebsch−Gordon coefficient (CGC).[31] Any component $h_{-m}(i)$ can be substituted for $f(i)$, and one obtains

$$\langle aS_aM|H'_{SOC}|bS_bM'\rangle = \sum_m (-1)^m \begin{pmatrix} S_b & 1 & S_a \\ M' & m & M \end{pmatrix} Y_{ab}^{S_aS_b}(-m) \tag{9}$$

where $Y_{ab}^{S_aS_b}(-m)$ denotes a reduced matrix element. The same equation in terms of density functions was given by McWeeny,[20b] and a closely analogous equation but with inclusion of the spatial symmetry contained in the vector operator h_{-m} by Griffith.[30] Since most of our future applications will be to systems with little or no symmetry, we disregard the spatial symmetry and use eq 9. The selection rules contained in the CGCs require $S_a - S_b = 0, \pm 1$, and the reduced matrix elements are calculated for the standard states with $M = S$, giving

(25) Löwdin, P.O. In *Pertubation Theory and its Applications in Quantum Mechanics*; Wilcox, C. H., Ed.; John Wiley and Sons Inc.: New York, 1966; pp 255ff.
(26) Weil, J. A.; Bolton, J. R.; Wertz, J. E. *Electron Paramagnetic Resonance. Elementary Theory and Practical Applications*; Wiley Interscience: New York, 1994.
(27) (a) Blume, M.; Watson, R. E. *Proc. R. Soc. A* **1962**, *270*, 127. (b) Blume, M.; Watson, R. E. *Proc. R. Soc. A* **1963**, *271*, 565. (c) Blume, M.; Freeman, A. J.; Watson, R. E. *Phys. Rev.* **1964**, *134*, A320.
(28) (a) McClure, D. S. *J. Chem. Phys.* **1952**, *20*, 682. (b) McGlynn, S. P.; Vanquickenborne, L. G.; Kinoshita, M.; Carroll, D. G. *Introduction to Applied Quantum Chemistry*; Holt, Rinehart, and Winston Inc.: New York, 1972. (c) Misetich A. A.; Buch T. *J. Chem. Phys.* **1964**, *41* (8), 2524.
(29) (a) Moores, W. H.; McWeeny, R. *Proc. R. Soc. A* **1973**, *332*, 365. (b) Abegg, P. W.; Ha, T. K. *Mol. Phys.* **1974**, *27* (3), 763. (c) Pasternak, R.; Wagniere, G. *J. Comput. Chem.* **1981**, *2* (3), 347. (d) Koseki, S.; Schmidt, M. W.; Gordon, M. S. *J. Chem. Phys.* **1992**, *96*, 10768. (e) Langhoff, S. R. *J. Chem. Phys.* **1974**, *61*, 1708. (f) Cohen, J. S.; Wadt, W. R.; Hay, P. J. *J. Chem. Phys.* **1979** *71*, 2955.
(30) Griffith, J. S. *The Irreducible Tensor Method for Molecular Symmetry Groups*; Prentice-Hall Inc.: Englewood Cliffs, NJ, 1962.
(31) Rose, M. E. *Elementary Theory of Angular Momentum*; Dover Publications Inc.: New York, 1957.
(32) Lushington, G. H.; Grein, F. *Theor. Chim. Acta* **1996**, *93*, 259.
(33) Ditchfield, R. *Mol. Phys.* **1974**, *27(4)*, 789.

$$Y_{ab}^{S_aS_a}(-m) = \frac{\sqrt{S_a(S_a+1)}}{S_a}\langle aS_aS_a|\sum_i h_{-m}(i)\, s_0(i)|bS_aS_a\rangle \quad (10)$$

$$Y_{ab}^{S_aS_a+1}(-m) = \sqrt{\frac{2S_a+3}{2S_a+1}}\langle aS_aS_a|\sum_i h_{-m}(i)\, s_{-1}(i)|b(S_a+1)(S_a+1)\rangle \quad (11)$$

$$Y_{ab}^{S_aS_a-1}(-m) = \langle aS_aS_a|\sum_i h_{-m}(i)\, s_{+1}(i)|b(S_a-1)(S_a-1)\rangle \quad (12)$$

The part of the second-order contribution, eq 5, that contains H'_{SOC} twice is

$$T_{MM'}^{(k)} = -\sum_{bM''}\Delta_b{}^{-1}\langle aS_aM|H'_{SOC}|bS_bM''\rangle\langle bS_bM''|H'_{SOC}|aS_aM'\rangle \quad (13)$$

where it is understood that the sum includes only the terms with $S_b = S_a + k$ ($k = 0, \pm1$). By inserting the appropriate matrix elements, the connection to the matrix elements of H_{ZFS},

$$\langle SM|H_{ZFS}|SM'\rangle = \sum_{m,m'}(-1)^{m+m'} D_{mm'}\sum_{M''}\langle SM|S_m|SM''\rangle \times \langle SM''|S_{m'}|SM'\rangle \quad (14)$$

can now be made (here $D_{mm'}$ is an element of the **D**-tensor in spherical components). Three cases need to be distinguished, relating to $S_a - S_b = 0, \pm1$.

2.3. Contributions with $S_b = S_a$. Insertion of eqs 9 and 10 into 13 yields

$$T_{MM'}^{(0)} = -\sum_{m,m'}(-1)^{m+m'}\sum_b \Delta_b{}^{-1} Y_{ab}^{S_aS_a}(-m)Y_{ba}^{S_aS_a}(-m') \times \sum_{M''}\begin{pmatrix} S_a & 1 & S_a \\ M'' & m & M\end{pmatrix}\begin{pmatrix} S_a & 1 & S_a \\ M' & m' & M''\end{pmatrix} \quad (15)$$

$$= -\frac{1}{S_a^2}\sum_{m,m'}(-1)^{m+m'}\sum_b \Delta_b^{-1} \times \langle aS_aS_a|\sum_i h_{-m}(i)\, s_0(i)|bS_bS_b\rangle\langle bS_bS_b|\sum_i h_{-m'}(i)\, s_0(i)|aS_aS_a\rangle \times \sum_{M''}\langle S_aM|S_m|S_aM''\rangle\langle S_aM''|S_{m'}|S_aM'\rangle$$

By comparing eqs 14 and 15, one obtains after switching back to Cartesian indices ($p, q = x, y, z$)

$$D_{pq}^{(0)} = -\frac{1}{S_a{}^2}\sum_b \delta_{S_aS_b}\Delta_b{}^{-1}\langle aS_aS_a|\sum_{A,i}\xi(r_{iA})\, l_{A,p}(i)\, s_0(i)|bS_bS_b\rangle \times \langle bS_bS_b|\sum_{A,i}\xi(r_{iA})\, l_{A,q}(i)\, s_0(i)|aS_aS_a\rangle \quad (16)$$

which is McWeeny's result,[20] using the Zeeman operator in the form

$$H_{ZE} = \beta_B\sum_i \vec{B}(\vec{l}(i) + g_e\vec{s}(i)) \quad (17)$$

The parts of the second-order energy that contain the products of matrix elements of H'_{SOC} and H_{ZE} yield the g-shift as[20]

$$\Delta g_{pq} = -\frac{1}{S_a}\sum_b \Delta_b{}^{-1}\delta_{S_aS_b}\{\langle aS_aS_a|\sum_i l_p(i)|bS_bS_b\rangle \langle bS_bS_b|\sum_{i,A}\xi(r_{iA})\, l_{A,q}(i)\, s_0(i)|aS_aS_a\rangle + \langle aS_aS_a|\sum_{i,A}\xi(r_{iA})\, l_{A,p}(i)\, s_0(i)|bS_bS_b\rangle\langle bS_bS_b|\sum_i l_q(i)|aS_aS_a\rangle\} \quad (18)$$

It is important to point out that the Zeeman operator has no matrix elements between states of different multiplicity (for $a \neq b$) and therefore to second order the **g**-matrix unlike the **D**-tensor contains no contributions from states with a total spin different from that of the ground state. This appears not generally to be recognized, as many treatments relate both the **D**- and the **g**-matrix to a common tensor Λ. As discussed in the literature,[5d,14,20,21,32] the evaluation of the orbital angular momentum matrix elements introduces a variance with respect to the choice of origin. Numerical calculations suggest that the effects are small if the center of charge is taken as origin.[32] Alternatively, gauge invariant angular momentum operators can be defined[20] or field-dependent atomic orbitals used (for example see ref 33 and references therein).

2.4. Contributions from States with $S_b = S_a \pm 1$. The importance of contributions of this type to ZFSs has been clearly recognized in the case of Cr(III)[15] and ^{6}S ground-state ions.[10,16,17,19] It is not obvious that the pertubation sum $T_{MM'}^{(k)}$ ($k = \pm1$) has the same MM' and mm' dependence as eq 14 when $S_b \neq S_a$. This however is the requirement for being able to write down a SH that is bilinear in the spin operators. Griffith[8c,10] has shown that this is possible, but his result was not in the standard form of eq 1. In this section a **D**-tensor in standard form is obtained. To proceed define $d_{mm'}^b$

$$d_{mm'}^b = -\Delta_b{}^{-1}Y_{ab}^{S_aS_b}(-m)\, Y_{ba}^{S_bS_a}(-m') \quad (19)$$

Consider first

$$T_{MM'}^{(1)} = \sum_{m,m'}(-1)^{m+m'}\sum_b d_{mm'}^b\sum_{M''}\begin{pmatrix} S_a+1 & 1 & S_a \\ M'' & m & M\end{pmatrix} \times \begin{pmatrix} S_a & 1 & S_a+1 \\ M' & m' & M''\end{pmatrix} \quad (20)$$

The selection rule is contained in the last sum. For the first CGC it is $M'' + m = M$ and for the second $M' + m' = M''$. These are the same selection rules as for the case $S_a = S_b$. However, the numerical value of the CGC is different in the present case, and a proportionality to the spin-only matrix elements of the form $\langle SM|S_m|SM'\rangle$ is not immediately evident. Consider a matrix element $\langle SM|H_{ZFS}|SM-2\rangle$ of the spin Hamiltonian:

$$\langle SM|H_{ZFS}|SM-2\rangle = {}^1/_2\sqrt{(S-M+1)(S+M)}\,\sqrt{(S-M+2)(S+M-1)}D_{11} \quad (21)$$

Alternatively, the pertubation sum gives

$$T^{(1)}_{MM-2} = \sum_b d^b_{11} \begin{pmatrix} S_a+1 & 1 & | & S_a \\ M-1 & 1 & | & M \end{pmatrix} \begin{pmatrix} S_a & 1 & | & S_a+1 \\ M-2 & 1 & | & M-1 \end{pmatrix} \quad (22)$$

$$= \sum_b d^b_{11} \frac{1}{\sqrt{2}} \times \frac{\sqrt{(S_a+M)(S_a+M-1)(S_a-M+1)(S_a-M+2)}}{\sqrt{(S_a+1)(2S_a+1)(2S_a+2)(2S_a+3)}}$$

Thus, the M dependence of the two matrix elements is the same, and it can therefore be concluded that they will be numerically equivalent if it is defined

$$D^{(1)}_{11} = \frac{\sqrt{2}}{\sqrt{(S_a+1)(2S_a+1)(2S_a+2)(2S_a+3)}} \sum_b d^b_{11} \quad (23)$$

The same proportionality is readily established for $D^{(1)}_{-1-1}$, $D^{(1)}_{01}$, $D^{(1)}_{10}$, $D^{(1)}_{0-1}$, and $D^{(1)}_{-10}$. Next, consider a diagonal element of the spin Hamiltonian:

$$\langle SM|H_{ZFS}|SM\rangle = M^2 D_{00} - {}^1/_2(S-M)(S+M+1)D_{-11} - {}^1/_2(S+M)(S-M+1)D_{1-1} \quad (24)$$

The perturbation sum gives

$$T^{(1)}_{MM} = \sum_b d^b_{00} \begin{pmatrix} S_a+1 & 1 & | & S_a \\ M & 0 & | & M \end{pmatrix} \begin{pmatrix} S_a & 1 & | & S_a+1 \\ M & 0 & | & M \end{pmatrix} + d^b_{-11} \begin{pmatrix} S_a+1 & 1 & | & S_a \\ M+1 & -1 & | & M \end{pmatrix} \begin{pmatrix} S_a & 1 & | & S_a+1 \\ M & 1 & | & M+1 \end{pmatrix} + d^b_{1-1} \begin{pmatrix} S_a+1 & 1 & | & S_a \\ M-1 & 1 & | & M \end{pmatrix} \begin{pmatrix} S_a & 1 & | & S_a+1 \\ M & -1 & | & M-1 \end{pmatrix} \quad (25)$$

$$= \frac{\sqrt{2}}{\sqrt{(S_a+1)(2S_a+1)(2S_a+2)(2S_a+3)}} \times \sum_b (S_a+M+1)(S_a-M+1)d^b_{00} + {}^1/_2(S_a+M+1)(S_a+M+2)d^b_{-11} + {}^1/_2(S_a-M+1)(S_a-M+2)d^b_{1-1}$$

Now the average of all eigenvalues of the SH is subtracted from each diagonal element. By means of the diagonal sum rule this average is equal to the average of the sum of the diagonal elements. Using

$$\frac{1}{2S+1} \sum_{M=-S}^{S} M^2 = {}^1/_3 S(S+1) \quad (26)$$

$$\frac{1}{2S+1} \sum_{M=-S}^{S} -{}^1/_2(S \mp M)(S \pm M + 1) = -{}^1/_3 S(S+1) \quad (27)$$

the corrected diagonal elements of the spin Hamiltonian become

$$\langle SM|H_{ZFS}|SM\rangle - \frac{1}{2S+1} \sum_{M'=-S}^{S} \langle SM|H_{ZFS}|SM\rangle = [M^2 - {}^1/_3 S(S+1)][D_{00} + {}^1/_2 D_{1-1} + {}^1/_2 D_{-11}] \quad (28)$$

The term linear in M cancels. For the perturbation sum the equivalent average is

$$\frac{1}{2S_a+1}\Bigg[\sum_{M=-S_a}^{S_a} \begin{pmatrix} S_a+1 & 1 & | & S_a \\ M & 0 & | & M \end{pmatrix} \begin{pmatrix} S_a & 1 & | & S_a+1 \\ M & 0 & | & M \end{pmatrix} \sum_b d^b_{00} + \sum_{M=-S_a}^{S_a} \begin{pmatrix} S_a+1 & 1 & | & S_a \\ M-1 & 1 & | & M \end{pmatrix} \begin{pmatrix} S_a & 1 & | & S_a+1 \\ M & -1 & | & M-1 \end{pmatrix} \sum_b d^b_{1-1} + \sum_{M=-S_a}^{S_a} \begin{pmatrix} S_a+1 & 1 & | & S_a \\ M+1 & -1 & | & M \end{pmatrix} \begin{pmatrix} S_a & 1 & | & S_a+1 \\ M & 1 & | & M+1 \end{pmatrix} \sum_b d^b_{-11} \Bigg] = -\frac{1}{3}\sqrt{\frac{2S_a+3}{2S_a+1}} [\sum_b d^b_{00} + d^b_{-11} + d^b_{1-1}] \quad (29)$$

Subtracting this from any diagonal element and taking into account the definition of the reduced matrix elements eqs 10−12, it is concluded that the contribution from states with $S_b = S_a + 1$ to the **D**-tensor is given by

$$D^{(1)}_{pq} = -\frac{1}{(S_a+1)(2S_a+1)} \times \sum_b \delta_{S_b S_a+1} \Delta_b^{-1} \langle aS_aS_a| \sum_{i,A} \xi(r_{iA})\, l_{A,p}(i)\, s_{-1}(i) |bS_bS_b\rangle \times \langle bS_bS_b| \sum_{i,A} \xi(r_{iA})\, l_{A,q}(i)\, s_{+1}(i) |aS_aS_a\rangle \quad (30)$$

where again p and q refer to the Cartesian components of the **D**-tensor. Repeating the process for excited states with $S_b = S_a - 1$ results in the following contribution to the **D**-tensor

$$D^{(-1)}_{pq} = -\frac{1}{S_a(2S_a-1)} \times \sum_b \delta_{S_b S_a-1} \Delta_b^{-1} \langle aS_aS_a| \sum_{i,A} \xi(r_{iA})\, l_{A,p}(i)\, s_{+1}(i) |bS_bS_b\rangle \times \langle bS_bS_b| \sum_{i,A} \xi(r_{iA})\, l_{A,q}(i)\, s_{-1}(i) |aS_aS_a\rangle \quad (31)$$

Summing up, the second-order contributions to the ZFS tensor from SOC are given by

$$D_{pq} = D^{(0)}_{pq} + D^{(1)}_{pq} + D^{(-1)}_{pq} \quad (32)$$

with the individual contributions given by eqs 16, 30, and 31.

2.5. Formulation in Terms of Molecular Orbitals. Having obtained general expressions for the elements of the **D**- and **g**-matrices, it remains to specify approximations to the many-electron wave functions appearing in eqs 16, 18, 30, and 31 in order to perform actual calculations. In this and in the next section we discuss two standard choices, namely, single determinants and CI type wave functions.

2.5.1. Spin-Restricted Determinants. The most elementary case is when all states $\{|\alpha S_\alpha M\rangle\}$ can be expressed as single Slater determinants. This is the case for certain restricted open shell HF (ROHF) solutions and related methods. If a wave function for spin S can be represented by a single normalized Slater determinant (denoted as $|...|$) with n doubly and m singly occupied orbitals, it is of the high-spin type:[34]

$$|0SS\rangle = |\psi_1\bar{\psi}_1 \ldots \psi_n\bar{\psi}_n\psi_{o_1} \ldots \psi_{o_m}| \quad (33)$$

An excited state in which an electron is promoted from a doubly occupied into one of the singly occupied MOs is also an

(34) $\bar{\psi}$ is an orbital that is occupied by a spin-down electron, while ψ is occupied by a spin-up electron.

eigenfunction to S^2 and S_z with the same eigenvalues:

$$|I_i^{o_j}SS\rangle = |\psi_1\bar{\psi}_1 \ldots \psi_i\bar{\psi}_{o_j} \ldots \psi_n\bar{\psi}_n\psi_{o_1} \ldots \psi_{o_m}| \quad (34)$$

Likewise, if an electron is promoted from one of the singly occupied orbitals into an empty orbital, a single-determinant spin eigenfunction is obtained:

$$|II_{o_i}^{a}SS\rangle = |\psi_1\bar{\psi}_1 \ldots \psi_n\bar{\psi}_n\psi_{o_1} \ldots \psi_a \ldots \bar{\psi}_{o_m}| \quad (35)$$

The case where an electron is promoted from a doubly occupied into an empty orbital is more complicated because it leads to several states of the same multiplicity as well as states of different multiplicities. The same is true for spin-flip states in which an electron is promoted from one of the singly occupied orbitals into another singly occupied orbital with an accompanying spin flip. These excitations give rise to several states of lower multiplicity than the ground state. In the latter two cases proceeding on a case by case basis is probably best. However, general conclusions can be drawn for the two types of excited-state wave functions in eqs 34 and 35. These wave functions are not in general accurate descriptions of the actual states, as they neglect excited-state electronic relaxation. They are useful however from a conceptional point of view as they link physical observables to individual MOs. Using Slater's rules[20,35] in eq 16 gives

$$\langle 0SS|\sum_{A,i}\xi(r_{iA})\, l_{A,p}(i)\, s_0(i)|I_i^{o_j}SS\rangle = -\frac{1}{2}\langle\psi_i|\sum_A\xi(r_A)l_{A,p}|\psi_{o_j}\rangle \quad (36)$$

$$\langle 0SS|\sum_{A,i}\xi(r_{iA})\, l_{A,p}s_0(i)|II_{o_i}^{a}SS\rangle = +\frac{1}{2}\langle\psi_{o_i}|\sum_A\xi(r_A)\, l_{A,p}|\psi_a\rangle \quad (37)$$

For real MOs these two matrix elements are purely imaginary and hermitian. Therefore the contributions of these two types of excited states to the **D**-tensor become

$$D_{pq}^{(0)} = -\frac{1}{4S^2}\left\{\sum_{i(\text{doubly})}\sum_{o_j(\text{singly})}\Delta_{I_i^{o_j}}^{-1}\bar{L}_{1p}^{io_j}\bar{L}_{1q}^{io_j} + \sum_{a(\text{virt})}\sum_{o_j(\text{singly})}\Delta_{I_{o_j}^{a}}^{-1}\bar{L}_{1p}^{o_ja}\bar{L}_{1q}^{o_ja}\right\} \quad (38)$$

where $\bar{L}_{1p}^{ij} \equiv \text{Im}(\langle\psi_i|\sum_A\xi(r_A)l_{A,p}|\psi_j\rangle)$. Note that $\bar{L}_{1p}^{ij} = -\bar{L}_{1p}^{ji}$. Using the same matrix elements, the **g**-matrix becomes

$$\Delta g_{pq} = +\frac{1}{2S_{i(\text{doubly})}}\sum_{o_j(\text{singly})}\Delta_{I_i^{o_j}}^{-1}\{\bar{L}_{2p}^{io_j}\bar{L}_{1q}^{io_j} + \bar{L}_{1p}^{io_j}\bar{L}_{2q}^{io_j}\} - \frac{1}{2S_{a(\text{virt})}}\sum_{o_j(\text{singly})}\Delta_{II_{o_j}^{a}}^{-1}\{\bar{L}_{2p}^{o_ja}\bar{L}_{1q}^{o_ja} + \bar{L}_{1p}^{o_ja}\bar{L}_{2q}^{o_ja}\} \quad (39)$$

where $\bar{L}_{2p}^{ij} \equiv \text{Im}(\langle(\psi_i|l_p|\psi_j\rangle)$. The positive sign for the first contribution arises from the s_0 term in the SOC operator. This is related to the fact that in order to create an excited state $|I_i^{o_j}SS\rangle$ a spin-down electron must be excited, while in order to create an excited state $|II_{o_j}^{a}SS\rangle$ a spin-up electron is excited. This accounts for the fact that d^1 systems have negative *g*-shifts while d^9 systems have positive *g*-shifts as long as only d−d transitions contribute to the *g*-shift (no low lying charge-transfer states). The same sign change does not occur for the **D**-tensor because each term in eq 16 contains s_0 twice.

2.5.2. Spin-Polarized Determinants. In a spin-polarized bonding scheme (spin-unrestricted DFT or HF) the ground-state determinant is written

$$|0SS\rangle = |\bar{\psi}_1^{\beta} \ldots \bar{\psi}_n^{\beta}\, \psi_1^{\alpha} \ldots \psi_{n+m}^{\alpha}| \quad (40)$$

where α refers to spin-up and β to spin-down electrons. Excited states are formed by replacing occupied spin-up or spin-down MOs with virtual MOs of the same spin:

$$|I_i^aSS\rangle = |\bar{\psi}_1^{\beta} \ldots \bar{\psi}_n^{\beta}\, \psi_1^{\alpha} \ldots \psi_{i-1}^{\alpha}\, \psi_a^{\alpha}\, \psi_{i+1}^{\alpha} \ldots \psi_{n+m}^{\alpha}| \quad (41)$$

and

$$|II_i^aSS\rangle = |\bar{\psi}_1^{\beta} \ldots \bar{\psi}_{i-1}^{\beta}\, \bar{\psi}_a^{\beta}\, \bar{\psi}_{i+1}^{\beta} \ldots \bar{\psi}_n^{\beta}\, \psi_1^{\alpha} \ldots \psi_{n+m}^{\alpha}| \quad (42)$$

Using these excited states, one first calculates the analogues of eqs 36 and 37 and then inserts into eqs 16 and 18 to obtain

$$D_{pq}^{(0)} = -\frac{1}{4S^2}\{\sum_{i(\alpha\text{-occ})}\sum_{a(\alpha\text{-virt})}\Delta_{I_i^a}^{-1}\bar{L}_{1p}^{i_\alpha a_\alpha}\bar{L}_{1q}^{i_\alpha a_\alpha} + \sum_{i(\beta\text{-occ})}\sum_{a(\beta\text{-virt})}\Delta_{II_i^a}^{-1}\bar{L}_{1p}^{i_\beta a_\beta}\bar{L}_{1q}^{i_\beta a_\beta}\} \quad (43)$$

and

$$\Delta g_{pq} = -\frac{1}{2S_{i(\alpha\text{-occ})}}\sum_{a(\alpha\text{-virt})}\Delta_{I_i^a}^{-1}\{\bar{L}_{2p}^{i_\alpha a_\alpha}\bar{L}_{1q}^{i_\alpha a_\alpha} + \bar{L}_{1p}^{i_\alpha a_\alpha}\bar{L}_{2q}^{i_\alpha a_\alpha}\} + \frac{1}{2S_{i(\beta\text{-occ})}}\sum_{a(\beta\text{-virt})}\Delta_{II_i^a}^{-1}\{\bar{L}_{2p}^{i_\beta a_\beta}\bar{L}_{1q}^{i_\beta a_\beta} + \bar{L}_{1p}^{i_\beta a_\beta}\bar{L}_{2q}^{i_\beta a_\beta}\} \quad (44)$$

Excitations from spin-up to spin-down MOs cannot easily be incorporated into the calculations because they would lead to nonorthogonal configurations. The problem with this approach is that the value *S* of the total spin is ill defined because the determinants in eqs 40, 41, and 42 are not spin eigenfunctions[35] and spin contamination may be much larger in the excited states than in the ground state.[36]

2.5.3. Matrix Elements over MOs. The matrix element involving MOs *i* and *j* is resolved into a sum of integrals over basis functions in eq 45,

$$\langle\psi_i|\sum_A\xi(r_A)l_{A,p}|\psi_j\rangle = \sum_{r,s}c_{ri}c_{sj}\langle\phi_r|\sum_A\xi(r_A)l_{A,p}|\phi_s\rangle \quad (45)$$

where the functions $\{\phi\}$ form the atomic orbital basis set and the *c*'s are the MO coefficients. This leads to one-, two-, and three-center integrals. The two- and three-center integrals may be neglected due to the r_A^{-3} dependence of the $\xi(r_A)$ operator, eq 6, and the one-center integrals are elementary to evaluate.[28b,37] To a good approximation,

$$\langle\psi_i|\sum_A\xi(r_A)l_{A,p}|\psi_j\rangle \approx \sum_A\sum_{r,s}c_{ri}c_{sj}\zeta_{rs}^A\langle\phi_r^A|l_{A,p}|\phi_s^A\rangle \quad (46)$$

with $\zeta_{rs}^A = \langle R_r^A|\xi(r_A)|R_s^A\rangle$ where $R_r^A(r)_A$ is the radial part of ϕ_r and the Kronecker delta is included to indicate that the integral

(35) Szabo, A.; Ostlund, N. S. *Modern Theoretical Chemistry*; MacMillan Pub. Inc.: New York, 1982.
(36) Bacon, A. D.; Zerner, M. C. *Theor. Chim. Acta* **1979**, *53*, 21.
(37) Mabbs, F. E.; Collison, D. *Electron Paramagnetic Resonance of d-Transition Metal Compounds*; Elsevier: Amsterdam, 1992.

vanishes if ϕ_r and ϕ_s have different angular momentum quantum numbers. The ζ_{rs}^{A} may either be approximated by the SOC constants of the appropriate free atoms or ions or be theoretically evaluated as considered in section 4.

2.6. Implementation in Terms of CI Wave Functions. A general and in principle rigorous way to construct the many-electron wave functions required in the evaluation of eqs 16, 18, 30, and 31 is the method of configuration interaction (CI). In a CI treatment each Born−Oppenheimer eigenfunction is constructed by a many-electron wave function of the form

$$|\alpha S_\alpha M\rangle = \sum_\gamma C_{\gamma\alpha}\Phi_\gamma \tag{47}$$

where usually $M = S_a$ and the coefficients C are assumed real. Each configuration state function (CSF) Φ_γ is an antisymmetric function in the electronic coordinates and consists of an orbital product built from a set of orthonormal MOs $\{\psi\}$ and a spin function. In the most basic case it is a single Slater determinant. Although expansions of up to more than 10^7 CSFs become practical[38] in practice, one usually has to work with a severely truncated set $\{\Phi\}$. The matrix element of any one-electron operator, $\hat{o}$, between two CSFs can be written

$$\langle \alpha S_\alpha S_\alpha | \sum_i \hat{o}(i) | \beta S_\beta S_\beta \rangle = \sum_{\gamma\delta} C_{\gamma\alpha} C_{\gamma\beta} \sum_{pq} \Gamma_{pq}^{\gamma\delta} \langle \psi_p | \hat{o} | \psi_q \rangle \tag{48}$$

where the coupling coefficients Γ depend on the way the functions $\{\Phi\}$ are constructed. A straightforward way to do this is the method of bonded functions.[20,39−42] Matrix elements between two bonded functions of the same S and spin-independent one- and two-electron operators were worked out by Boys and Reeves,[39] Sutcliffe,[40] and Cooper and McWeeny.[41] Summaries can be found in the books by McWeeny[20] and Pauncz.[42] A computer program to carry out the projective reduction was reported by Reeves,[43] and computational strategies for CI calculations based on bonded functions have been discussed.[44] The case of spin-dependent one-electron operators was treated by Manne and Zerner[45] and applied to SOC calculations by Kotzian et al.[46] Our present implementation of the theory is based on this formulation with MOs determined by semiempirical valence-only methods like the INDO/S model of Zerner and co-workers[36,47] and atomic SOC constants.[48−50] The coefficients Γ are evaluated together with the Hamiltonian matrix elements during the CI calculation and stored in an external file. For $S_a \neq S_b$ Reeves's algorithm[43] cannot be used to determine the Γ coefficients, and a special procedure was developed following Manne and Zerner.[45] To evaluate the **D**-tensor and the **g**-matrix, this file need only be read once, and for each set of indices p, q, γ, and δ the contributions of each pair of states 0, α to the sum in eqs 16, 30, and 31 are evaluated. Finally, the full **D**-tensor is found by performing the appropriate sums. The **g**-matrix is evaluated according to eq 18 at the same time, as this requires negligible extra effort. The number of contributing states is defined by either the number of eigenvectors available from the CI calculation or a given excited-state energy threshold above which the contributions are supposed to be too small to warrant evaluation. After the **D**-tensor is evaluated, it is diagonalized and the combination of eigenvectors determined that define a proper coordinate system. On the basis of this choice the D and E/D values are assigned.

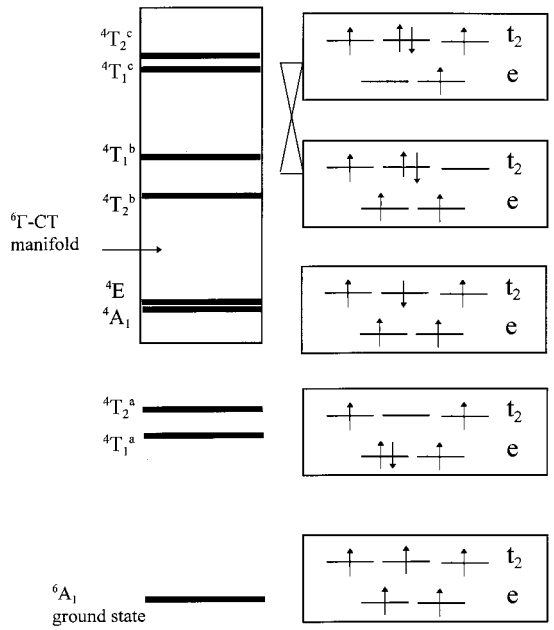

Figure 1. Energy levels of a high-spin ferric ion on a cubic ligand field.

3. Application to High-Spin Ferric Complexes

The equations given above are general and include all situations that are likely to be met in practice except for the case of ground-state orbital degeneracy where a spin Hamiltonian approach is not appropriate. This development was driven by our interest in ferric-active sites in non-heme iron enzymes. Together with the development of a general MCD theory to be presented elsewhere,[51] the present methodology constitutes a powerful probe of the electronic and geometric structure of these sites. It is therefore appropriate at this point consider the factors that govern the ZFS in high-spin ferric complexes with $FeCl_4^-$ taken as an illustrative example since it has been studied in detail.[16,17]

3.1. Approximate Expressions for the ZFSs of High-Spin Ferric Complexes. The low lying electronic states typically found in cubic high-spin d^5 systems follow from ligand field theory and are shown in Figure 1. In the $^6A_1$ ground state

(38) Siegbahn, P. E. M. In *Lecture Notes in Quantum Chemistry*; Roos, B. O., Ed.; Springer: Berlin, 1992; pp 255ff.
(39) Boys, S. F.; Reeves, C. M.; Shavitt, I. *Nature* **1956**, *178*, 1207.
(40) Sutcliffe, B. T. *J. Chem. Phys.* **1966**, *45*, 235.
(41) Cooper, I. L.; McWeeny, R. *J. Chem. Phys.* **1966**, *45*, 226.
(42) Pauncz, R. *Spin Eigenfunctions. Construction and Use*; Plenum Press: New York, 1979.
(43) Reeves, C. M. *Commun. ACM* **1966**, *9*, 276.
(44) (a) Roos, B.O. In *Computational Techniques in Quantum Chemistry and Molecular Physics*; Diercksen, G. H. F., et al., Eds.; D. Reidel Pub. Inc.: Dordrecht, Holland, 1975; pp 251ff. (b) Scott, J. M.; Sutcliffe, B. T. *Theor. Chim. Acta* **1975**, *39*, 289. (c) Diercksen, G. H. F.; Sutcliffe, B. T. *Theor. Chim. Acta* **1974**, *34*, 105.
(45) Manne, R.; Zerner, M. C. *Int. J. Quantum Chem. Symp.* **1986**, *19*, 165.
(46) Kotzian, M.; Rösch, N.; Zerner, M. C. *Int. J. Quantum Chem. Symp.* **1991**, *25*, 545.
(47) (a) Ridley, J.; Zerner, M. C. *Theor. Chim. Acta* **1973**, *32*, 111. (b) Zerner, M. C.; Loew, G. H.; Kirchner, R. F.; Mueller-Westerhoff, U. T. *J. Am. Chem. Soc.* **1980**, *102*, 589. (c) Anderson, W. P.; Edwards, W. D.; Zerner, M. C. *Inorg. Chem.* **1986**, *25*, 2728.
(48) Edlen, B. *Encycl. Phys.* **1964**, *80*.
(49) Bendix, J.; Brorson, M.; Schäffer, C. E. *Inorg. Chem.* **1993**, *32*, 2838.
(50) Dunn, T. M. *Trans. Faraday Soc.* **1961**, *57*, 1441.
(51) Neese, F.; Solomon, E. I. Submitted for publication.
(52) This result is due to the configurational mixing between the $^4T_1$ states following from the $(e^2t_2{}^3)$ and the $(e^1t_2{}^4)$ configurations. The large contribution from the $^4T_1{}^b$ state in Table 1 actually comes from the $(e^1t_2{}^4)$ character in this state.

(denoted $|0\rangle$) there are five singly occupied MOs of mainly Fe 3d character, and a single-determinantal wave function of the high-spin type, eq 33, is a reasonable representation for this state. Since there are no spin-allowed transitions within the d set the first excited states have quartet multiplicity with a pair of $^4T_1$ and $^4T_2$ states being lowest.[53] To higher energies a series of quartet states follow that usually partially overlap with the onset of sextet LMCT states in which an electron is promoted from a mainly ligand-centered MO to one of the singly occupied Fe 3d based MOs. If the quartet states were all represented by single determinants of the form

$$|\psi_{o_i} \rightarrow \bar{\psi}_{o_j}\rangle = |\psi_1\bar{\psi}_1 \ldots \psi_n\bar{\psi}_n\psi_{o_1} \ldots \bar{\psi}_{o_j} \ldots \psi_{o_5}| \quad (49)$$

the contribution of these states to the ZFS could be easily calculated because

$$\langle 0|\sum_{A,i}\xi(r_{iA})\, l_{A,p}(i)\, s_{+1}(i)|\psi_{o_i} \rightarrow \bar{\psi}_{o_j}\rangle = -\frac{1}{\sqrt{2}}\langle\psi_{o_i}|\sum_{A}\xi(r_A)l_{A,p}|\psi_{o_j}\rangle = -\frac{1}{\sqrt{2}}\bar{L}_{1p}^{o_io_j} \quad (50)$$

therefore from eq 31

$$D_{pq}^{(-1)} = \left(-\frac{1}{{}^5/_2(2^5/_2 - 1)}\right)\left(-\frac{1}{2}\right)\sum_{o_i,o_j}\Delta_{o_i\rightarrow\bar{o}_j}^{-1}\bar{L}_{1p}^{o_io_j}\bar{L}_{1q}^{o_io_j} = \frac{1}{20}\sum_{o_i,o_j}\Delta_{o_i\rightarrow\bar{o}_j}^{-1}\bar{L}_{1p}^{o_io_j}\bar{L}_{1q}^{o_io_j} \quad (51)$$

In section 4.3 of the paper we will make the connection between MO and ligand field theory and show that the integrals L_{1p}^{ij} can be obtained from eq 45 without introducing further approximations as

$$L_{1p}^{ij} = \zeta_{Fe}\,\mathrm{Im}(\langle d_i|l_{Fe,p}|d_j\rangle)K_{ij}^p \quad (52)$$

where $|d_i\rangle$ is the Fe 3d part of MO i, K_p^{ij} is to be interpreted as a generalized orbital reduction factor that includes the ligand SOC and a variety of other effects, and ζ_{Fe} is a suitably (but arbitrarily) chosen free-ion SOC constant. Accordingly, eq 51 becomes

$$D_{pq}^{(-1)} = \frac{\zeta_{Fe}^2}{20}\sum_{o_i,o_j}\Delta_{o_i\rightarrow\bar{o}_j}^{-1}K_{o_io_j}^pK_{o_io_j}^q\,\mathrm{Im}(\langle d_{o_i}|l_{Fe,p}|d_{o_j}\rangle)\,\mathrm{Im}(\langle d_{o_i}|l_{Fe,q}|d_{o_j}\rangle) \quad (53)$$

However, single determinants are usually not suitable approximations to the excited quartet ligand field states, and a more complete consideration of $D_{pq}^{(-1)}$ in high-spin ferric complexes is necessary.

3.1.1. Contributions from the Lowest Quartet State. In cubic symmetry the ground state $^6A_1$ state can only spin−orbit couple to states of T_1 symmetry. In a distorted tetrahedral molecule the lowest $^4T_1$ is dominated by the t → e excitations that are represented by

$$|^4T_{1z}^a\rangle = |\psi_{xy} \rightarrow \bar{\psi}_{x^2-y^2}\rangle \quad (54a)$$

$$|^4T_{1x}^a\rangle = \cos\eta|\psi_{yz} \rightarrow \bar{\psi}_{x^2-y^2}\rangle + \sin\eta|\psi_{yz} \rightarrow \bar{\psi}_{z^2}\rangle \quad (54b)$$

$$|^4T_{1y}^a\rangle = \cos\eta|\psi_{xz} \rightarrow \bar{\psi}_{x^2-y^2}\rangle - \sin\eta|\psi_{xz} \rightarrow \bar{\psi}_{z^2}\rangle \quad (54c)$$

with $\eta = \pi/3$. Using these states in eq 31 together with eqs 50 and 52, one finds for the ZFS

$$D(^4T_1^a) = \frac{\zeta_{Fe}^2}{20}\left[\frac{4(K_{xy,x^2-y^2}^z)^2}{E(^4T_{1z}^a)} - \frac{1}{8}\left(\frac{(K_{yz,x^2-y^2}^x + 3K_{yz,z^2}^x)^2}{E(^4T_{1x}^a)} + \frac{(K_{xz,x^2-y^2}^y + 3K_{xz,z^2}^y)^2}{E(^4T_{1y}^a)}\right)\right] \quad (55)$$

Let us assume for the moment that the K's can be factored into contributions belonging to individual MOs, i.e., $K_{ij}^p \approx \alpha_i\alpha_j$. In perfectly cubic environments symmetry demands that the energy denominators are equal and also $\alpha_{xy} = \alpha_{xz} = \alpha_{yz}$ and $\alpha_{x^2-y^2} = \alpha_{z^2}$, i.e., $D(^4T_1^a) = 0$. Nonzero contributions in lower symmetries can be mainly traced back to two sources, namely, distortions that lift the degeneracy of the three quartet states and changes in covalencies of individual MOs that reflect differences in bonding interactions.

3.1.2. Contributions from Low-Symmetry Distortions. Let us initially assume that all K's are equal to 1 and that the distortion splits the quartet states in a manner consistent with ligand field theory:

$$E(^4T_{1z}^a) = E_0 + {}^1/_2\Delta_e + {}^1/_2\Delta_{t_2} \quad (56a)$$

$$E(^4T_{1x,y}^a) = E_0 + {}^1/_4\Delta_e - {}^1/_2\Delta_{t_2} \quad (56b)$$

Here Δ_e is positive if $\psi_{x^2-y^2}$ is above ψ_{z^2}, Δ_{t_2} is positive if $\psi_{xz,yz}$ is above ψ_{xy}, and $E_0^{(a)}$. Using the series $(a + b)^{-1} = \sum_i(-1)^ib^ia^{-i-1}$, which converges rapidly for $b \ll a$, one arrives at a contribution to D from this mechanism that is given by

$$D(^4T_1^a)_{dist} \cong -\frac{1}{5}\left(\frac{\zeta_{Fe}}{E_0^{(a)}}\right)^2[\Delta_e + {}^3/_4\Delta_{t_2} - {}^1/_4\Delta_e\Delta_{t_2}/E_0^{(a)}] \quad (57)$$

Thus, if Δ_e is small, this approximation, which is essentially the same as Griffith's,[19] suggests that D would be positive if $\psi_{xz,yz}$ is below ψ_{xy} (flattened tetrahedron) and negative if $\psi_{xz,yz}$ is above ψ_{xy} (compressed tetrahedron).

3.1.3. Contributions from Anisotropic Covalency. To see the effect of covalency, one might assume $\alpha_{x^2-y^2} \approx \alpha_{z^2} = \alpha$, $\alpha_{xy} = \delta$, and $\alpha_{xz} = \alpha_{yz} = \gamma$. Equation 57 is then modified to

$$D(^4T_1^a)_{cov} \cong \frac{1}{5}\frac{\zeta_{Fe}^2}{E_0^{(a)}}\alpha^2[\delta^2(1 - {}^1/_2x_e - {}^1/_2x_{t_2} + {}^1/_2x_ex_{t_2}) - \gamma^2(1 + {}^1/_2x_e + {}^1/_4x_{t_2} + {}^1/_4x_ex_{t_2})] \quad (58)$$

with $x_e = \Delta_e/E_0^{(a)}$ and $x_{t_2} = \Delta_{t_2}/E_0^{(a)}$. For the typical case of negative x_{t_2} and small x_e one can also expect $\delta^2 < \gamma^2$, and therefore in this case the effect of covalency on the ZFS is negative while the distortion gives a positive contribution.

3.1.4. Contributions from Higher Quartet States. This situation changes for the higher lying $^4T_1$ states. $^4T_1^c$ is mainly composed of the e → t excitations that give rise to states with analogous determinantal descriptions. The only difference is that now Δ_e and Δ_{t_2} change sign because the one-electron energy is

(53) Sugano, S.; Tanabe, Y.; Kamimura, H. *Multiplets of Transition Metal Ions in Crystals*; Academic Press: New York, 1970.

increased in the excited state. Therefore the contribution from $^4T_1^c$ is

$$D(^4T_1^c)_{cov} \cong \frac{1}{5}\frac{\zeta_{Fe}^2}{E_0^{(b)}}\alpha^2[\delta^2(1 + {}^1/_2x'_e + {}^1/_2x'_{t_2} + {}^1/_2x'_ex'_{t_2}) - \gamma^2(1 - {}^1/_2x'_e - {}^1/_4x'_{t_2} + {}^1/_4x'_ex'_{t_2})] \quad (59)$$

with $x'_e = \Delta_e/E_0^{(c)}$ and $x'_{t_2} = \Delta_{t_2}/E_0^{(c)}$. It is important to note that for $^4T_1^c$ the covalency and distortion contributions work in the same direction; that is, for negative x'_{t_2}, small x'_e, and $\delta^2 < \gamma^2$ the effects of both covalency and distortion are negative. Thus, although $^4T_1^c$ is typically $>10\,000$ cm^{-1} higher in energy than $^4T_1^a$, it is likely to make a significant contribution to the ZFS.

The third $^4T_1$ state, $^4T_1^b$, is dominated by the spin-flip transitions within the t_2-set. It does not split to first order with a geometric distortion but has a small contribution to the ZFS arising from anisotropic covalency:

$$D(^4T_1^b) = \frac{1}{10}\zeta_{Fe}^2\gamma^2\left[\frac{\gamma^2}{E(^4T_{1z}^b)} - \frac{\delta^2}{E(^4T_{1x,y}^b)}\right] \quad (60)$$

3.1.5. Change of States with Distortion. If a geometric distortion, say $T_d \rightarrow D_{2d}$, is present, it cannot necessarily be expected that the states in eq 54 retain the same determinantal composition. From group theory $^4T_1^a$ splits into $^4A_2$ and $^4E^a$, while $^4T_2^a$ splits into $^4B_2$ and $^4E^b$. Of these states $^4B_2$ cannot spin−orbit couple with the $^6A_1$ ground state, $^4A_2$ spin−orbit couples via the *z*-component, while the ^4E states couple via the *x*,*y* components of the SOC operator. Furthermore, the two ^4E states are allowed to mix by CI. The $^4A_2$ and $^4E_x^a$ and $^4E_y^a$ states are represented by eqs 54a−c, and the $^4B_2$ and $^4E^b$ states are given by

$$|^4B_2\rangle = |\psi_{xy} \rightarrow \bar{\psi}_{z^2}\rangle \quad (61a)$$

$$|^4E_x^b\rangle = -\sin\eta|\psi_{yx} \rightarrow \bar{\psi}_{x^2-y^2}\rangle + \cos\eta|\psi_{yz} \rightarrow \bar{\psi}_{z^2}\rangle \quad (61b)$$

$$|^4E_y^b\rangle = \sin\eta|\psi_{xz} \rightarrow \bar{\psi}_{x^2-y^2}\rangle + \cos\eta|\psi_{xz} \rightarrow \bar{\psi}_{z^2}\rangle \quad (61c)$$

The CI effect is described by a deviation of the angle η from its tetrahedral value $\pi/3$. Writing $\eta = \pi/3 + \eta'$ and performing a power series expansion in η', the contributions of the $^4A_2$ and $^4E^a$ states are now

$$D^{(-1)}(^4T_1^a) = \frac{\zeta_{Fe}^2}{5}\alpha^2\left[\frac{\delta^2}{E(^4A_2)} - \gamma^2\frac{(1 - \eta'^2 + {}^1/_3\eta'^4)}{E(^4E^a)}\right] \quad (62)$$

Similarly, $^4E^b$ yields the contribution

$$D^{(-1)}(^4T_2^a) = -\frac{\zeta_{Fe}^2}{5}\alpha^2\gamma^2\frac{(\eta'^2 - {}^1/_3\eta'^4)}{E(^4E^b)} \quad (63)$$

Defining $\kappa = 1 - \eta'^2 + {}^1/_3\eta'^4$ (η' measured in radians), the two contributions can be combined to give

$$D^{(-1)}(^4T_1^a + {}^4T_2^a) = \frac{\zeta_{Fe}^2}{5}\alpha^2\left[\frac{\delta^2}{E(^4A_2)} - \gamma^2\left\{\frac{\kappa}{E(^4E^a)} + \frac{1-\kappa}{E(^4E^b)}\right\}\right] \quad (64)$$

An approximate expression is obtained using $t \equiv E(^4E^b) - E(^4E^a)$.

$$D^{(-1)}(^4T_1^a + {}^4T_2^a) \cong \frac{\zeta_{Fe}^2}{5}\alpha^2\left[\frac{\delta^2}{E(^4A_2)} - \frac{\gamma^2}{E(^4A^a)}\left\{1 - (1-\kappa)\left(\frac{t}{E(^4E^a)} - \frac{t^2}{E(^4E^a)^2}\right)\right\}\right] \quad (65)$$

The CI effect is now entirely contained in the term in {...}. For small angles, κ is close to 1 so that the effect of the CI is seen to be a small correction that can be included in the apparent value for γ^2. Thus, ignoring the CI effect will lead to a slight underestimate of the value of γ^2. However, in the numerical calculations on $FeCl_4^-$ to be presented below we find η' to be $\leq 5^\circ$, which gives an apparent reduction of γ^2 of only $\approx$0.1%.

3.1.6. Influence of CT States. The contribution of the spin sextet LMCT states can be estimated from eq 38. These contributions are best calculated numerically for a specific case.

3.1.7. Influence of Ligand SOC. Finally we want to explicitly include the ligand SOC in the calculation. As will be shown later K_{ij}^p in eq 52 must simply be multiplied by a factor $K_{ij}^{p,lig}$. If four equal ligands are assumed and for simplicity overlap is neglected,

$$K_{xy,x^2-y^2}^{z,lig} \approx 1 - {}^1/_2\nu_L\sqrt{(1-\delta^2)/\delta^2}\,\sqrt{(1-\alpha^2)/\alpha^2} \quad (66a)$$

$$K_{yz,x^2-y^2}^{x,y,lig} = K_{yz,z^2}^{x,y,\mathrm{lig}} \approx 1 - {}^1/_2\nu_L\sqrt{(1-\gamma^2)/\gamma^2}\,\sqrt{(1-\alpha^2)/\alpha^2} \quad (66b)$$

($\nu_L = \zeta_L/\zeta_{Fe}$). Inserting these factors into eq 55 gives explicit expressions of the additional ligand contributions to the $^4T_1^a$ terms in the ZFS expressions. There are terms linear and quadratic in ν_L. The linear terms vanish in the limits of either full ($\alpha = \gamma = \delta = 0$) or no ($\alpha = \gamma = \delta = 1$) covalency and therefore depend on the simultanous presence of ligand and metal SOC. The terms quadratic in ν_L are ligand-only in character and vanish only in the limit of no covalency.

3.1.8. Extension to Distorted Octahedral Sites. The case of octahedral sites is slightly more complicated because the anisotropic covalency pattern will differ from the tetrahedral case. Here it may be assumed $\alpha_{x_2-y_2} = \alpha$, $\alpha_{z^2} = \beta$, and $\alpha_{xz} = \alpha_{yz} = \alpha_{xy} = \gamma$. Instead of eq 58, the contribution from $^4T_{1g}^a$ is now given by

$$D(^4T_{1g}^a) = \frac{3}{80}\frac{\zeta_{Fe}^2}{E_0}\gamma^2[(\alpha-\beta)(5\alpha+3\beta) + \alpha^2({}^{17}/_6x_{t_{2g}} + {}^{11}/_4x_{e_g} + {}^{31}/_{12}x_{t_{2g}}x_{e_g}) + \beta^2({}^3/_2x_{t_{2g}} + {}^3/_4x_{e_g} - {}^3/_4x_{t_{2g}}x_{e_g}) + \alpha\beta(x_{t_{2g}} + {}^1/_2x_{e_g} - {}^1/_2x_{t_{2g}}x_{e_g})] \quad (67)$$

Again, for the typical case of small $x_{t_{2g}}$, positive x_{e_g}, and $\alpha^2 < \beta^2$ one has a negative contribution to the *D*-value from anisotropic covalency and a positive from the low-symmetry distortion. The contribution from $^4T_{1g}^c$ is given by the same equation with the signs of $x_{t_{2g}}$ and x_{e_g} reversed.

3.2. Numerical Results for $FeCl_4^-$. To probe the relative importance of the various contributions to ZFS, ROHF-INDO/S-CI calculations were carried out for $FeCl_4^-$ as a function of a distortion from T_d to D_{2d} symmetry using the SOC constants $\zeta_{Fe} = 397$ cm^{-1} and $\zeta_{Cl} \approx 550$ cm^{-1} that will be obtained in section 4.

The results in Figure 2 show that the ZFS is a nearly linear function of the distortion angle in the range $\pm10^\circ$ and that it contains significant contributions from both the ligand field and

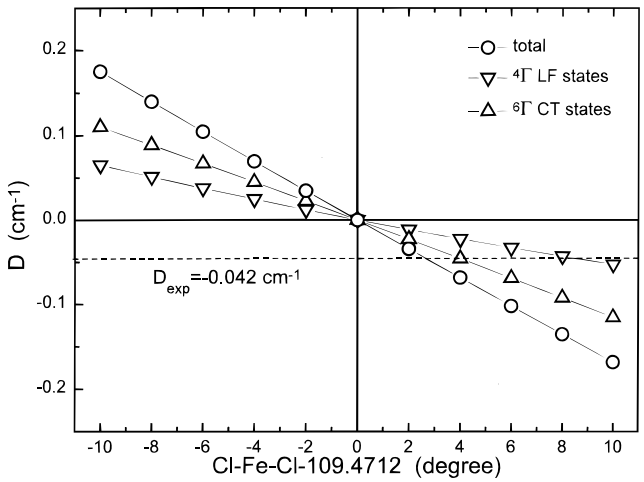

Figure 2. Calculated D-value for $FeCl_4^-$ as a function of the $T_d \rightarrow D_{2d}$ distortion angle and charge-transfer and ligand-field contributions.

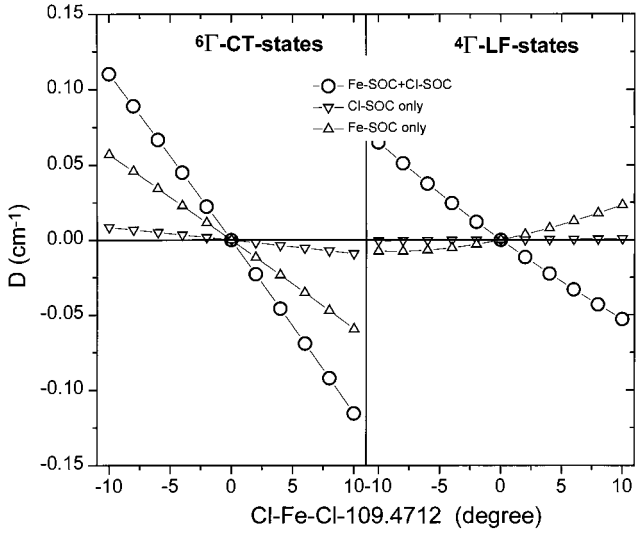

Figure 3. Breakdown of charge-transfer (left) and ligand-field (right) contributions to the total ZFS in $FeCl_4^-$ into metal SOC only and ligand SOC only contributions.

the charge-transfer excited states. The experimental value, $D = -0.042$ cm^{-1},[16,17] is reproduced at a distortion angle of $+2.7^\circ$ compared to an experimental angle of $+5.1^\circ$ at room temperature.[16,17] Since the deviation from cubic symmetry is small and the ZFS arises as the small difference of several contributions, better agreement cannot be expected. It is however significant that the calculations predict the correct sign and order of magnitude of the ZFS at the experimental distortion angle.

Figure 3 shows the combined $^6\Gamma$ and $^4\Gamma$ contributions separated into contributions to metal-only and ligand-only SOC. For both sets of states it is observed that the ligand-only contribution to the ZFS is quite small. Despite this, the ligand SOC is important, as can be seen from the difference between the metal-only and total contributions. This means that the terms linear in ν_{Cl}, i.e., proportional to $\zeta_{Cl}\zeta_{Fe}$, are important. For the CT states they have the same sign as the metal contributions, while for the LF contributions they have opposite sign. Explicit evaluation of the ligand reduction factors gives $K^{z,lig}_{xy,x^2-y^2} = 0.969$, $K^{x,lig}_{yz,x^2-y^2} = 0.976$, and $K^{x,lig}_{yz,z^2} = 0.974$. Thus in absolute terms the ligand contribution is quite small, but since it is anisotropic, it shifts the balance of terms that very nearly cancel each other if ligand SOC is neglected (Table 1). The more biologically relevant N- and O-containing ligands have much smaller spin−orbit coupling constants than chlorine ($\nu_{Cl} \approx 1.38$, whereas $\nu_{N,O} \leq 0.25$), covalency is usually more limited, and the ZFS is much larger. Consequently the ligand SOC effects will not nearly be as prominent as for $FeCl_4^-$. Much like the contributions of the anisotropic covalency to the metal contribution to the ZFS, the ligand contributions are negative and oppose those induced by the geometric distortion (eq 57), the latter being the only contributions taken into account in Griffith's model of ZFS.[19]

The breakdown of LF contributions to the ZFS in $FeCl_4^-$ in Table 1 shows that the contributions from $^4T_1^a$ and $^4T_1^b$ are comparable in magnitude and opposite in sign, while that of $^4T_1^c$ is much smaller.[52] It also follows from Table 1 that Griffith's model gives a large contribution of the wrong sign. Compared to the earlier analysis,[16,17] the CT contribution is calculated to be slightly less negative. The results for the first ligand-field excited state are also similar, while the balance of contributions from $^4T_1^b$ and $^4T_1^c$ is slightly changed. The MO coefficients found from the ROHF-INDO/S calculation are $\alpha^2 = 0.963$, $\delta^2 = 0.850$, and $\gamma^2 = 0.865$. Thus, as expected the σ-antibonding MOs are much more covalent than the π-antibonding MOs. Compared to the earlier X_α-SW results,[16,17] both the π- and σ-covalencies are calculated to be smaller, with a more pronounced difference for the π-value (0.963 compared to 0.840 from X_α-SW).[16,17]

In conclusion, the present calculations are largely consistent with the previous analysis and experimental results for $FeCl_4^-$ and demonstrate the usefulness of the method in the modeling of ZFS. The extremely important role of covalency for the ZFS is emphasized. The anisotropy in the covalency not only induces contributions of opposite sign of those induced by low-symmetry ligand field splittings but also leads to the appearance of charge transfer and ligand SOC contributions that are both found to be important.

4. Change of Metal Radial Functions: Contributions to the Relativistic Nephelauxetic Effect

There are three main factors that contribute to the apparent reduction of the metal SOC constant in complexes: (a) the covalent mixing of metal and ligand orbitals (the symmetry-restricted covalency in Jørgensen's nomenclature[9]), (b) the ligand spin−orbit coupling, and (c) the change in metal radial wave function that leads to values of ζ_{rs} in eq 45 that are different from the free-ion values (the central field covalence[9]). To evaluate ζ_{rs} using the operator in eq 6, one needs to know the radial functions of the contributing atomic orbitals. Explicit electronic structure calculations are reported in this section to estimate how these radial functions change upon going from the free ion to the complex.

4.1. Free-Ion Calculations. Based on eq 6 a linear relationship is expected between ζ_{3d} for a given ion and the respective $\langle r^{-3}\rangle_{3d}$ values. Therefore, we first evaluate this proportionality by comparing calculated $\langle r^{-3}\rangle_{3d}$ values with experimentally determined ζ_{3d}'s for Fe ions with different d^n configurations. The 3d radial distribution functions from spin-averaged Hartree−Fock[54] calculations using a relatively large basis set of Slater orbitals are displayed in Figure 4 for n varying from 2 to 7 and show the expected increase in diffuseness with decreasing positive charge of the ion. Since the Hartree−Fock approximation is well-known to produce one-electron expectation values

(54) (a) Stavrev, K. K.; Zerner, M. C. *Int. J. Quantum Chem.* **1997**, *65*, 877. (b) Edwards, W. D.; Zerner, M. C. *Theor. Chem. Acta* **1987**, *72*, 347. (c) Zerner, M. C. *Int. J. Quantum Chem.* **1989**, *XXXV*, 567.

Table 1. Contributions of Excited States to the ZFS in $FeCl_4^-$ at a Distortion Angle of 2.7° As Calculated by the ROHF-INDO/S-CI Method[e]

state	E_{calc}[a]	D_{total} (cm^{-1})	$D_{Griffith}$ (cm^{-1})	D_{metal} (cm^{-1})	D_{lig} (cm^{-1})	D_{mixed} (cm^{-1})
$^4T_1$[a]	15 100 ($^4A_2$) 15 773 (^4E)	+0.070	+0.089	+0.086	+0.001	−0.017
$^4T_1$[b,b]	24 582 (^4E) 24 990 ($^4A_2$)	−0.077[c]	−0.021	−0.078	0.000	+0.001
$^4T_1$[c,b]	30 666 (^4E) 31 027 ($^4A_2$)	−0.009	−0.006	−0.002	−0.001	−0.006
$^4\Gamma$ total		−0.016	+0.055	+0.005	0.000	−0.022
$^6\Gamma$ total		−0.031[d]		−0.016	−0.002	−0.013
total		−0.047	+0.062	−0.011	−0.002	−0.035
exptl		−0.042				

[a] Note that these numbers cannot be directly compared to the experimental transition energies since the experimental numbers in contrast to the theoretical ones contain spin−orbit coupling. [b] There is considerable configurational mixing among the $^4T_1{}^b(e^2t^3)$ and $^4T_1{}^c(e^1t^4)$ states. [c] This number contains a -0.012 cm^{-1} contribution from the ^4E state following from $^4T_2{}^b$. [d] This number contains contributions from many states. There is a significant amount of electronic relaxation in the CT excited states of $FeCl_4^-$ that will be analyzed elsewhere. [e] $D_{Griffith}$ = considering the low-symmetry distortions only. D_{metal} = contributions of metal SOC alone. D_{lig} = contributions of ligand SOC alone. $D_{mixed} = D_{total} - D_{metal} - D_{lig}$.

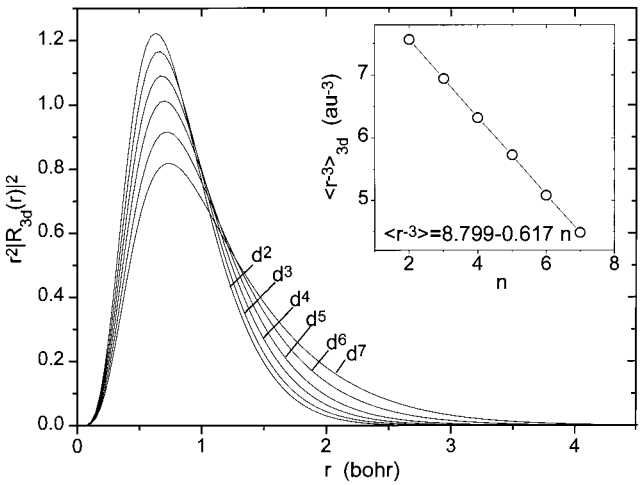

Figure 4. Free-ion 3d radial distribution function for Fe ions with different d^n configurations found from spin-averaged Hartree−Fock calculations.

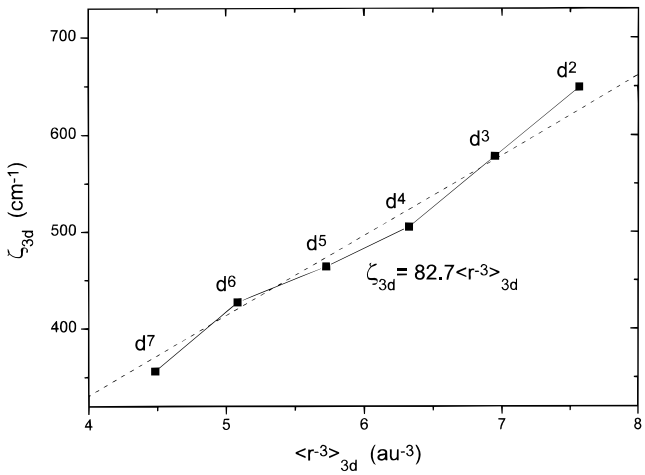

Figure 5. Correlation of empirically determined spin−orbit coupling constants for Fe ions with different d^n configurations[49] and calculated radial expectation values $\langle r^{-3}\rangle_{3d}$.

that are correct to second order, the radial expectation values from these calculations are quite accurate. For the $\langle r^{-3}\rangle_{3d}$ value an almost exact linear dependence on the number of 3d electrons is found (inset to Figure 4). This slightly contrasts with Slater's rules that predict a cubic dependence but with very small coefficients for the quadratic and cubic terms. The empirical correlation of the $\langle r^{-3}\rangle_{3d}$ values with the experimental ζ_{3d} values determined by Bendix et al.[49] is shown in Figure 5. A correlation coefficient of 0.993 and a standard deviation of 15.7 cm^{-1} are obtained. From the slope the reasonable value $Z_{eff} = 14.0$ is calculated for the Fe 3d electrons, compared to $Z_{eff} = 13.2$ from Slater's rules.[55] This accuracy is sufficient to make useful predictions about the variation of the SOC constants found in molecules based on calculated radial distribution functions.

Since molecular Hartree−Fock calculations are not yet feasible with a basis set of Slater orbitals, the calculations were repeated for Fe(III) with a basis of Gaussian orbitals and the basis was enlarged up to the point where the Slater orbital values for $\langle r^{-3}\rangle_{3d}$ were reproduced to ≈1% accuracy. In addition to the UHF method, the B3LYP hybrid density functional model[56] was employed. This method is presently thought to be one of the most accurate electronic structure models and effectively incorporates dynamic correlation effects that are absent in the Hartree−Fock model. The values found for d^5 from UHF and B3LYP calculations for $\langle r^{-3}\rangle_{3d}$ are similar (5.669 vs 5.738 au^{-3}).

4.2. Calculations on $FeCl_4^-$. The same Gaussian basis was then employed in molecular calculations on T_d $FeCl_4^-$ at the UHF, ROHF, spin-polarized- (UB3LYP), and spin-restricted (RB3LYP) B3LYP levels. The metal 3d parts of the five singly occupied MOs were evaluated along one of their lobes and renormalized, and the $\langle r^{-3}\rangle_{3d}$ values were determined by numerical integration (Table 2). Here we will discuss only the RB3LYP results.[57]

Figure 6 shows the iron radial probability distribution functions that were obtained for the singly occupied metal-based t_2 and e MOs together with the corresponding functions for the free Fe(I), Fe(II), and Fe(III) ions. The radial functions for the complex are seen to be considerably more diffuse than those of the Fe(III) ion and are in fact intermediate between those for Fe(I) and Fe(II). Importantly there is an increased probability in the outer valence region that increases the metal−ligand overlap and aids in the formation of covalent bonds. On average

(55) Atkins, P. W. *Molecular Quantum Mechanics, 2nd ed.*; Oxford University Press: Oxford, 1983.

(56) (a) Becke, A. D. *Phys. Rev. A* **1988**, *38*, 3098. (b) Becke, A. D. *J. Chem. Phys.* **1993**, *98*, 1372. (c) Becke, A. D. *J. Chem. Phys.* **1993**, *98*, 5648.

(57) The UB3LYP functions are very similar to the RB3LYP ones, while the ROHF and UHF functions are more intermediate between the Fe(II) and Fe(III) functions, consistent with the trends in Table 2 and the general notion that the HF description of the bonding in transition metal complexes is too ionic.

(58) Watson, R. E.; Freeman, A. J. In *Hyperfine Interactions*; Freeman, A. J., Frankel, R. B., Eds.; Academic Press: New York, 1967; pp 53ff.

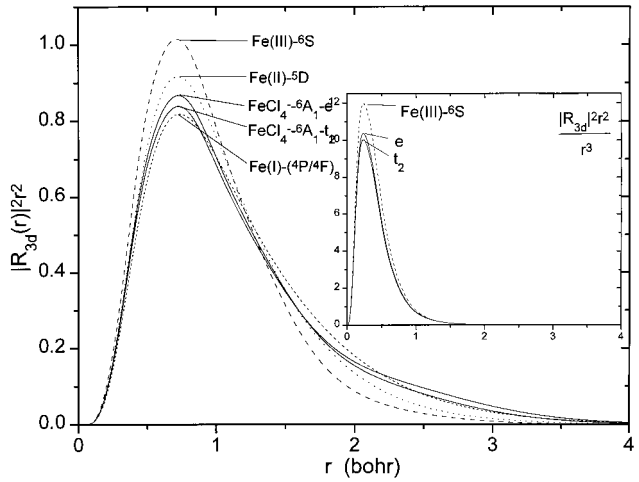

Figure 6. Comparison of free-ion Fe 3d radial distribution functions with those calculated for the metal-based t_2 and e MOs of $FeCl_4^-$ by the RB3LYP method. Inset: Graphical illustration of the $\langle r^{-3}\rangle_{3d}$ found for the complex. $\langle r^{-3}\rangle_{3d}$ is equal to the area under each curve.

the reduction of the $\langle r^{-3}\rangle_{3d}$ values found in the calculations is ≈15% (Table 2). Thus the effect is sizable and should not be neglected. Interestingly there is also some anisotropy found in the values obtained for the t_2 and e MOs. If the physical origin of the effect would simply be a reduction in the effective nuclear charge felt by the Fe 3d electrons due to electron donation by the ligands, an isotropic reduction would result.[59] This discrepancy is related to a fundamental aspect of chemical bonding that will be taken up in the discussion. In applications to tetrahedral $FeCl_4^-$ the matrix element $\langle e|r^{-3}|t_2\rangle$ is also of concern. These values are also given in Table 2 and are roughly intermediate between the expectation values for the t_2 and e MOs.

4.3. Connection to Ligand-Field Theory. In this section an equation is given that allows one to consider the factors that contribute to the total reduction in the apparent metal SOC constant that is commonly invoked in ligand-field treatments. The equation can be viewed as an anisotropic generalization of Stevens' orbital reduction factor,[8b,60] although it explicitly contains symmetry-restricted covalency, central field covalency, and ligand SOC. Initially the SOC constant of the free metal ion (ζ_{ion}) is factored out of eq 45:

$$\langle\psi_i|\sum_A \xi(r_A) l_{A,p}|\psi_j\rangle = \zeta_{ion}\sum_A\sum_{r,s}^{A} c_{ri}c_{sj}\delta_{l,l_s}(\zeta_{rs}^A/\zeta_{ion})\langle\phi_r^A|l_{A,p}|\phi_s^A\rangle \quad (68)$$

To simplify the following discussion, a typical nonzero matrix element is considered under the following assumptions: (a) the metal contributes only the d orbitals $|d_r^M\rangle$ and $d_s^M\rangle$ to MOs i and j, (b) every ligand contributes at most a single p orbital $|p_r^L\rangle$ to MO i and $|p_s^L\rangle$ to MO j, and (c) in crystal field theory the matrix element would be given by $\zeta_{ion}l_{ij}^p$.

$$\psi_i = a_{ri}|d_i^M\rangle + \sum_L b_{ri}^L|p_r^L\rangle + \eta_i \quad (69)$$

η_i symbolizes the remaining contributions of s orbitals that do not contribute to the SOC matrix elements. Equation 68 can then be factored as follows:

$$\langle\psi_i|\sum_A \xi(r_A) l_{A,p}|\psi_j\rangle = \zeta_{ion}l_{ij}^p K_{ij}^p = \zeta_{ion}l_{ij}^p K_{ij}^{src} K_{ij}^{cfc} K_{ij}^{p,lig} \quad (70)$$

where

$$K_{ij}^{src} = a_{ri}a_{sj} \quad (71)$$

$$K_{ij}^{cfc} = \zeta_{rs}^{Fe}/\zeta_{ion} \quad (72)$$

$$K_{ij}^{p,lig} = 1 + \sum_L P_{ri,sj}^L \frac{\zeta_{rs}^L}{\zeta_{rs}^{Fe}}\left|\frac{b_{ri}^L b_{sj}^L}{a_{ri}a_{sj}}\frac{\langle p_r^L|l_{L,p}|p_s^L\rangle}{l_{rs}^p}\right| \quad (73)$$

Equation 70 expresses the anisotropic reduction of the metal SOC constant by three factors: (a) $K_{ij}^{p,src}$ is the symmetry-restricted covalency where the reduction is stronger the less metal character contained in MOs i and j and the effect is also sensitive to metal−ligand and ligand-ligand overlap via the normalization conditions,[14f,60] (b) $K_{ij}^{p,cfc}$ is the central field covalence and describes the change of metal radial wavefunction upon complex formation as described in the previous section, and (c) $K_{ij}^{p,lig}$ describes the effect of the ligand SOC. The phase factor $P_{ri,sj}^L$ that governs the sign of the ligand contribution is sketched in Figure 7. It is equal to −1 if both ligand parts are either bonding or antibonding to the metal orbitals and +1 otherwise. It arises from the fact that the orbital angular momentum of the ligand is opposite that of the metal for antibonding MOs, while it is in the same direction for bonding MOs. Thus, the ligand contribution to a matrix element between a σ-antibonding MO and a π-antibonding MO is negative, while it is positive with a π-bonding MO (i.e., in a situation where L is π-back-bonding or in CT states where the donor orbital has significant M−L bonding character). Clearly, the importance of ligand contributions increases with increasing covalent bonding and increasing ligand SOC constant, but for many common donor ligands the effect will be small. We will return to the interpretation of the individual quantities in the discussion.

4.4. Contributions to the Relativistic Nephelauxetic Effect in $FeCl_4^-$. We are now in a position to give numbers for the contributions to the K_{pq} values in eq 70. To this end we list the percentage metal-d character in the t_2 and e MOs of $FeCl_4^-$ found by the various theoretical methods in Table 3.[61] The results show the typical trends found in calculations on transition metal complexes. Namely, the Hartree−Fock results show a much larger ionic character than the DFT results, especially for the π type interactions. From the RB3LYP results, the symmetry-restricted covalency factor, $K_{t_2,e}^{spc}$, is ≈0.78; that is, it accounts for 22% reduction of the metal SOC constant. From

(59) In spin-polarized calculations the spin-up Fe 3d orbitals are fully occupied and therefore contribute nothing to covalent bonding, while the unoccupied spin-down Fe 3d like orbitals are physically meaningless and lead to unreasonable results. The occupied bonding spin-down counterparts are mainly ligand in character. This effect has been discussed in detail by Watson and Freeman.[58] In the spin-polarized picture, the spin density around the iron is governed by the difference between a completely filled spin-up 3d shell and a partially covalent spin-down 3d shell, and the two shells are allowed to indivdually adjust their radial expansion. On the other hand, in the spin-restricted method the whole spin density is described by the five metal-based open shell MOs that therefore have to be covalent to give a realistic description. Consequently the radial functions of these orbitals lack the freedom to individually adjust and display the net radial expansion effect due to covalency more directly. In INDO/S calculations the UHF and ROHF wave functions have virtually identical energies.

(60) Gerloch, M.; Miller, J. R. *Prog. Inorg. Chem.* **1968**, *10*, 1.

(61) Here we have neglected the relatively small overlap charges in the metal-based t_2 and e MOs and only integrated over the Fe 3d part of the wave function.

Table 2. $\langle r^{-3}\rangle_{3d}$ for Metal-Based MOs in $FeCl_4^-$ Calculated by Various Quantum Mechanical Methods[a]

	$\langle Fe-3d_{t_2}\|r_{Fe}^{-3}\|Fe-3d_{t_2}\rangle$	$\langle Fe-3d_e\|r_{Fe}^{-3}\|Fe-3d_e\rangle$	$\langle Fe-3d_{t_2}\|r_{Fe}^{-3}\|Fe-3d_e\rangle$
ROHF	5.352 (93%)	5.313 (93%)	5.332 (93%)
UHF	5.194 (92%)	5.216 (92%)	5.205 (92%)
RB3LYP	4.736 (82%)	4.892 (85%)	4.813 (84%)
UB3LYP	4.759 (83%)	4.767 (83%)	4.763 (83%)

[a] Values in parentheses are % reduction relative to the free-ion values calculated at the same level of theory. For spin-polarized models the spin-up orbital values are quoted.

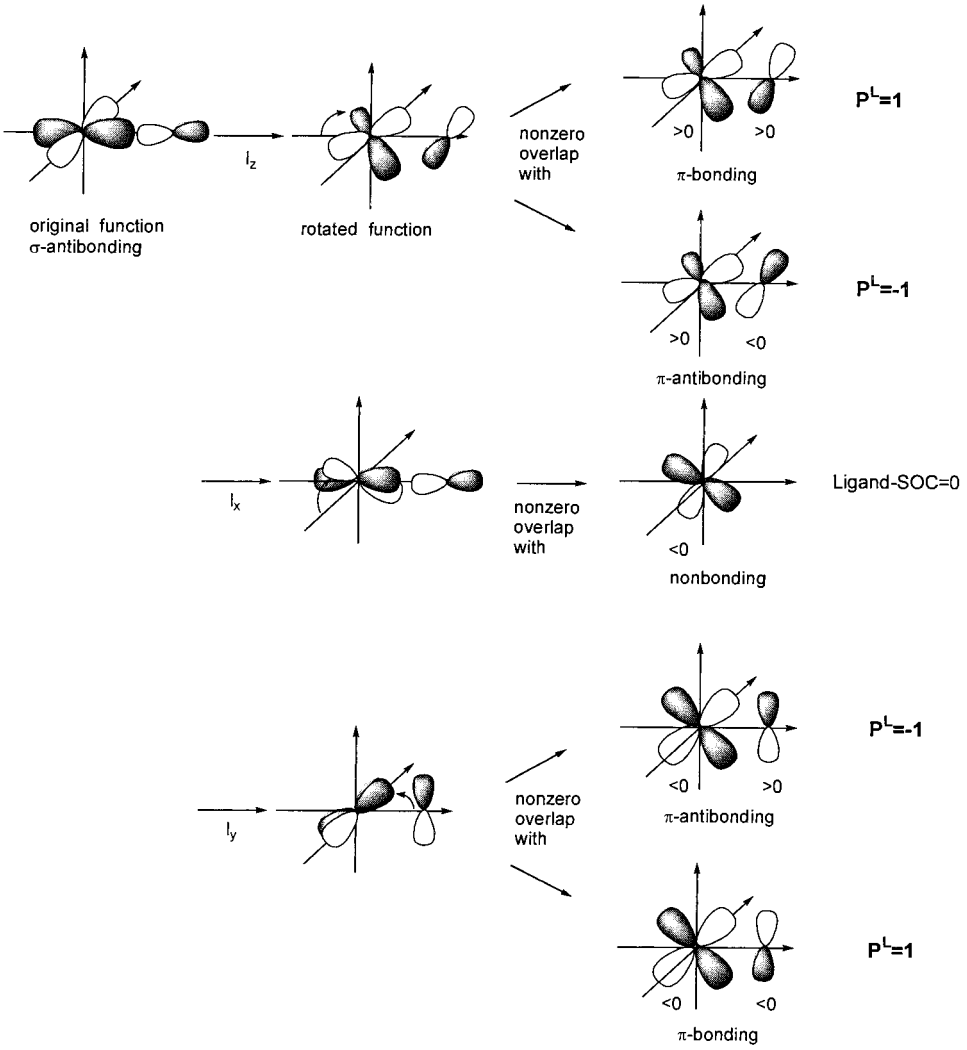

Figure 7. Illustration of the phase factors P^L.

Table 3. Fe 3d Character in the Metal-Based MOs of $FeCl_4^-$ As Calculated by Various Quantum Mechanical Methods[a]

	%Fe 3d t_2[b]	%Fe 3d e
ROHF	89.5	97.1
UHF	96.6	98.1
RB3LYP	70.2	86.6
UB3LYP	79.4	82.8
ROHF-INDO/S	83.2	96.3

[a] For spin-polarized models the spin-up orbital values are quoted. [b] Note that the p character in these MOs is <1% and does not affect our conclusions.

Table 2, the central field covalence, $K_{t_2,e}^{cfc}$, is slightly smaller and accounts for an additional 15% reduction. On the basis of the analysis of Bendix et al.,[49] this means that a value of $\zeta_{3d} \approx 397$ cm^{-1} is more appropriate if one works with fixed SOC constants.[62] However, this value cannot be expected to be transferable between different complexes but will depend on the intimate details of the chemical bonds formed between the metal and the ligands, as will be pointed out in the discussion.

While the INDO/S calculations showed a small but important ligand SOC effect of 4−5%, the RB3LYP method tends to give more weight to this term, basically because the π-covalency is predicted to be much larger than by the HF and INDO/S methods. In the special case of $FeCl_4^-$, the RB3LYP value for $K_{t_2,e}^{lig}$ is ≈0.82. As discussed above the ligand SOC effect will usually be much smaller in complexes with predominantly N and O ligation. Taken together, RB3LYP predicts a total reduction of the Fe 3d SOC constant to ≈54% of its free-ion value. While this reduction appears excessively large, it may be compared to the reduction of the Racah *B*-parameter in $FeCl_4^-$ that amounts to ≈54% of its free-ion value based on the position of the ligand-field exicted ^{4}E state.[17] The coinci-

(62) On the basis of the more commonly used value for the ferric ion SOC constant (430 cm^{-1}), one would obtain $\zeta_{3d} \approx 365$ cm^{-1}.

dence of these numbers is certainly fortuitous since the physical mechanisms that govern them are different, but the large reduction of B suggests that a similarly large reduction in ζ_{3d} is not unreasonable.

5. Discussion

5.1. Methodological Aspects. In this study a general and practical approach to the calculation of ZFSs and **g**-values in transition metal complexes was outlined. The inclusion of excited states of multiplicity different than the ground state makes the theory more general than previous treatments.[20] The main restriction is that an orbitally nondegenerate ground state is required, consistent with the use of a spin Hamiltonian (for example see ref 22). A typical example is provided by distorted octahedral, monuclear Fe(II) complexes where the ground state is a barely split $^5T_{2g}$ term, and a reasonable approach is to calculate the magnetic response of the system by diagonalization of a Hamiltonian that operates in the $^5T_{2g}$ manifold.[63]

One advantage of the formulation given in eqs 16, 18, 30, and 31 is that it makes no specific assumption about the type of wave function that is appropriate to describe the system under investigation. It is therefore applicable from the most elementary crystal field to the most sophisticated ab initio calculations and well suited to calculate **g**-matrices and **D**-tensors in complicated bonding situations where single-determinant wave functions are inappropriate. All that is required for the calculation is to formulate appropriate approximations to the ground- and excited-state wave functions for the standard choice $M = S$ and to evaluate at most three matrix elements between the ground and each excited state.

Treatments for g-values[14a] or second-order hyperfine couplings[14e] are frequently based on single-determinant (or single-configuration) states and therefore neglect electronic relaxation in electronically excited states, which is often large in the excitation and ionization spectra of transition metal complexes.[64] CI is a natural and straightforward way to describe this relaxation, and the present treatment is readily applied to CI wave functions. Relaxation shows up in CI calculations as a mixing of CSFs for different electronic configurations so that more than one pair of MOs contribute to a given matrix element between two states in eq 48.[66] Although the method of bonded functions was used in this work, the methodology described here is certainly not restricted to this type of CI calculation, and alternative approaches to the inclusion of SOC in CI calculations have been described in the literature.[29,67]

Some attempts to use density functional theory (DFT) to compute g-values and second-order hyperfine couplings have been reported for d^1 and d^9 systems[68] and also for iron−sulfur clusters.[69] In these calculations excited-state electronic relaxation was neglected. Incompletely solved problems in the application of DFT methods to second-order properties such as the **D**-tensors and **g**-matrices include (a) the excited states are not orthogonal to each other and the ground state when calculated by ΔSCF procedures, (b) the DFT wave functions are not eigenfunctions of the S^2 operator, and (c) the DFT single-determinantal wave functions do not in general describe multiplet splittings correctly. A promising alternative approach to sum over states methods is to include the relativistic effects in the self-consistent-field step, namely, within a coupled perturbed Hartree−Fock approach[20,70] or the zeroth-order regular approximation to the Dirac equation.[71]

The model outlined here was used in conjunction with the semiempirical INDO/S-SCF-MO-CI method[36,47] to gain insight into the electronic structure and properties of the active sites of several mononuclear non-heme iron enzymes and synthetic complexes that model these sites. It has been succesful in reproducing the sign, magnitude, and rhombicity of the ZFS. Similarly, the g-values of several Cu(II) complexes were calculated by the same method with reasonable results.[72] It is however important to check the validity of the approach by simultanously calculating the absorption spectrum of the compound under investigation. Without reasonably accurate transition energies, the energy denominators will give rise to large errors and any agreement of the calculated **g**-matrices and **D**-tensors with experimental values would be accidental. In this context it must be remarked that what is measured are the perturbed state energies, i.e. including SOC, while the theory in principle requires the energies of the unperturbed Born−Oppenheimer states. The difference may not be large in complexes of the first transition row (several hundred cm^{-1}), but is another potential source of uncertainty in the analysis.

5.2. The ZFS in High-Spin Ferric Complexes. In the second part of the paper we have discussed in some detail the subtleties involved in the calculation of ZFS in high-spin ferric complexes. The ZFS arises from a balance of several effects of opposing sign and contains contributions from low-symmetry ligand-field splittings, anisotropic covalency, charge-transfer states, and ligand SOC. It is especially important to realize the important role of covalency in these calculations. Ligand-field theory will frequently lead to qualitatively wrong results with regard to sign and magnitude of the ZFS. Covalency not only alters the balance between the terms entering the ZFS but also leads to the appearance of charge-transfer and ligand SOC contributions to the ZFS that can be quite sizable as we have found here for $FeCl_4^-$. Importantly, the ZFS is sensitive to differences in the covalencies of individual MOs, and therefore an average

(63) Solomon, E. I.; Pavel, E. G.; Loeb, K. E.; Campochiaro, C. *Coord. Chem. Rev.* **1995**, *144*, 370.
(64) (a) Butcher, K. D.; Didziulis, S. V.; Briat, B.; Solomon, E. I. *J. Am. Chem. Soc.* **1990**, *112*, 2231. (b) Butcher, K. D.; Gebhard, M. S.; Solomon, E. I. *Inorg. Chem.* **1990**, *29*, 2067. (c) Didziulis, S. V.; Cohen, S. L.; Gewirth, A. A.; Solomon, E. I. *J. Am. Chem. Soc.* **1988**, *110*, 250.
(65) Shavitt, I. In *Methods of Electronic Structure Theory*; Schaefer, H. F. III, Ed.; Plenum Press: New York, 1977; pp 189ff.
(66) If the excited state is still dominated by a given configuration, the effect of the CSF mixing can be interpreted as a change in the MOs that are principally involved in the excitation. This is particularly evident if approximate natural orbitals[65] for the excited states are calculated by diagonalizing the first-order density matrix for a given state. The advantage of the CI method over ΔSCF calculations is that despite the presence of relaxation, all excited states remain orthogonal to the ground state and to other excited states.
(67) (a) Hess, B. A.; Marian, C. M.; Peyerimhoff, S. D. In *Modern Electronic Structure Theory*; Yarkony, D. R., Ed.; 1995; pp 152ff. (b) Buenker, R. J.; Alekseyev, A. B.; Liebermann, H. P.; Lingott, R.; Hirsch, G. *J. Chem. Phys.* **1998**, *9*, 3400. (c) Morokuma, K.; Yamashita, K.; Yabushita, S. In *Supercomputer Algorithms for Reactivity Dynamics and Kinetics of Small Molecules*; Lagana, A., Ed.; Kluwer Acad. Pub.: Dordrecht, Holland, 1989; pp 37ff. (d) Karwowski, J. In *Methods in Computational Molecular Physics*; Diercksen, G. H. F., Wilson, S., Eds.; Plenum Press: New York, 1992; pp 65ff. (e) Sjovoll, M.; Gropen, O.; Olsen, J. *Theor. Chem. Acc.* **1997**, *97*, 301. (f) Ågren, H.; Vahtras, O.; Manev, B. *Adv. Quantum Chem.* **1996**, *27*, 71.
(68) (a) Geurts, P. J. M.; Bouten, P. C. P.; van der Avoird, A. *J. Chem. Phys.* **1980**, *73*, 1306. (b) Balagopalakrishna, C.; Kimbrough, J. T.; Westmoreland, T. D. *Inorg. Chem.* **1996**, *35*, 7758. (c) Deeth, R. J. *J. Chem. Soc., Dalton Trans.* **1991**, 1467.
(69) Noodleman, L.; Baerends, E. J. *J. Am. Chem. Soc.* **1984**, *106*, 2316.
(70) Kim, Y. S.; Lee, S. Y.; Oh, W. S.; Park, B. H.; Han, Y. K.; Park, S. J.; Lee, Y. S. *Int. J. Quantum Chem.* **1998**, *66*, 91.
(71) (a) van Lenthe, E.; Snijders, J. G.; Baerends, E. J. *J. Chem. Phys.* **1996**, *105* (15), 6505. (b) van Lenthe, E.; Wormer, P. E. S.; van der Avoird, A. *J. Chem. Phys.* **1997**, *107* (7), 2488. (c) Van Lenthe, E.; van der Avoird, A.; Wormer, E. S. *J. Chem. Phys.* **1998**, *108*, 4783.
(72) Neese, F. Dissertation, Universität Konstanz, 1997.

effective modeling of covalency with a uniform reduction of the SOC constant or a single Stevens orbital reduction factor will not be appropriate. In addition, the ZFS of distorted cubic high-spin ferric complexes will in general not be dominated by the contribution from the lowest $^4T_1$ state since for this state the contributions from low-symmetry distortions and anisotropic covalency tend to cancel each other.

5.3. The Relativistic Nephelauxetic Effect. On the basis of the discussion in section 4 there are three main factors contributing to the apparent reduction in the metal SOC constant required to explain experimental data, which are (a) the symmetry-restricted covalency that is directly related to the covalent mixing of the metal and ligand orbitals, (b) the central field covalency that is related to the change of the metal radial wave functions upon complex formation, and (c) the ligand SOC. Of these, (c) will usually be smallest unless the covalency is particular high and the ligand SOC constants are very large, as is the case for ligands beyond the first transition series. The metal SOC constants are almost invariably fixed at their free-ion values in the analysis of spin Hamiltonian data, and all reduction is attributed to symmetry-restricted covalency. This is the basis of methods that extract MO coefficients from magnetic resonance data. Often the case of Cu(II), where the SOC constant changes from 817 cm^{-1} to 828 cm^{-1} between Cu(0) and Cu(II), is invoked to imply negligible charge dependence of these values. However, this argument is misleading because the two configurations involved are $3d^9 4s^2$ and $3d^9 4s^0$ and the shielding effect of 4s on 3d electrons is very small.

The main point of section 4 is that the change in metal radial wave function is in fact not negligible compared to the symmetry-restricted covalency. Thus, MO coefficients extracted from spin Hamiltonian data will have a tendency to overestimate the metal−ligand covalent mixing if free-ion values are used for the expectation values of operators that depend on the metal radial wave functions, in particular $\langle r^{-3}\rangle_{3d}$. According to the calculations presented in section 4, a reduction of up to ≈15% in $\langle r^{-3}\rangle_{3d}$ can be expected for the metal-based antibonding MOs. However, this reduction may be different for different MOs, showing that there is more involved than just a uniform reduction in the effective nuclear charge felt by the 3d electrons due to charge donation by the ligands. The origin effect has been studied with considerable insight by Ammeter[73] and can be understood from Rüdenberg's analysis of the chemical bond.[74] According to this theory the destructive overlap in antibonding MOs leads to an increased gradient of the MO in the bonding region and consequently raises the kinetic energy.[75] The atomic orbitals involved will therefore tend to expand to decrease the potential energy in order to satisfy the virial theorem ($2\langle T\rangle = -\langle V\rangle$). The opposite is true for bonding MOs, where the atomic orbitals will contract. While this argument is only strictly valid for a one-electron system, the expansion/contraction effect is usually also found for individual MOs in many-electron systems[73] and therefore appears to be an important aspect of chemical bonding. Although the anisotropy of the $\langle r^{-3}\rangle_{3d}$ reduction was found to be limited in the present calculations (≈3% out of ≈15%), this need not always be the case, and more examples need to be considered before the typical magnitude of the effect can be fully appreciated.

A second point to be recognized is that the *g*-values will be more strongly affected than the *D*-values by the ligand angular momentum that opposes the metal 3d contribution in antibonding orbitals. The Zeeman matrix elements that involve the ligand angular momentum, eq 18, are not quenched by the R^{-3} dependence of the SOC operator and the small SOC constant of the ligands. In Ammeter's analysis of *g*-values of a series of Cu(II) complexes this effect accounts for up to 20% reduction in the *g*-shift.[73] This provides a rationale for the finding[15] that the interpretation of *g*- and *D*-values in some Cr(III) complexes required substantial reduction of the free-ion SOC constant in the case of *g*- but not in the case of *D*-values.

Finally it should be noted that the **D**-tensor contains contributions from states of different multiplicity than the ground state, whereas the **g**-matrix does not. Thus these two quantities cannot be related to a common tensor Λ, as frequently done in the literature.

Taken together the theory outlined here offers a general and practical approach to the interpretation of **D**- and **g**-matrices in transition metal complexes. It can be applied to any level of theory, and when combined with a suitable model of the compound under investigation, it provides an important link between theory and experiment and helps to assess the validity of the theoretical approach.

6. Computational Details

The spin-averaged Hartree−Fock calculations were carried out according to the formalism developed by Zerner and co-workers[54] and the program Orca developed by F.N. A 9s5p4d basis of Slater functions (STOs) was employed and all exponents were optimized for each ion by a quasi Newton procedure until the gradient was smaller than 2×10^{-4} hartree/bohr^{-1}. HF and B3LYP calculations with Gaussian orbitals (GTOs) were then carried out for Fe(III) using the Gaussian94 program.[76] For these calculations the d shell in the standard 6-311G basis set was fully uncontracted, and a Gaussian with exponent 0.25 was added to the s, p, and d sets. To compare radial expectation values to the STO values, a small program was written to read the Gaussian output file, project the degenerate components onto pure spherical harmonics, and evaluate the expectation values. The energy of the GTO-UHF wave function was higher than that of the corresponding STO-UHF one by ≈2.3 eV, but the expectation values agreed to ≈1%. The same basis set was then used in the molecular calculations on T_d $FeCl_4^-$. In these calculations a bond length of 2.195 Å was chosen and tight convergence requested (SCF = Tight). The metal parts of given MOs were then evaluated over a radial grid of 256 points and renormalized and expectation values calculated numerically. The ROHF-INDO/S-CI calculations for $FeCl_4^-$ were also carried out with the program Orca. Calculations were tightly converged on the $^6A_1$ ground state. The active space in the following Rumer diagram CI on the spin sextets consisted of all single excitations into the singly occupied MOs and from the singly occupied into the virtual MOs. For the spin quartets the 24 states that can be formed within the d manifold were included. In the **D**-tensor evaluation all states up to 60 000 cm^{-1} were taken into account.

Acknowledgment. Our research is supported by the National Institutes of Health (GM40392). F.N. thanks the Deutsche Forschungsgemeinschaft for a postdoctoral fellowship, Prof. Peter Kroneck (Konstanz) for support during his time in Konstanz, where part of developments reported here were made, and Dr. Thomas Brunold for helpful comments on an early version of the manuscript.
IC980948I

(73) Ammeter, J. *Chimia* **1968**, *22*, 469; Dissertation Eidgenössische Technische Universität Zürich, 1969.
(74) (a) Rüdenberg, K. *Rev. Mod. Phys.* **1962**, *34*, 326. (b) Feinberg, M. J.; Rüdenberg, K.; Mehler, E. L. *Adv. Quantum Chem.* **1970**, *5*, 27. (c) Feinberg, M. J.; Rüdenberg, K. *J. Chem. Phys.* **1971**, *59*, 1495.
(75) The kinetic energy of an electron in an orbital ψ is proportional to the average gradient of ψ squared, $KE \propto \int(\nabla\psi)^2 d^3r$.
(76) Frisch, M. J.; Trucks, G. W.; Schlegel, H. B.; Gill, P. M. W.; Johnson, B. G.; Robb, M. A.; Cheeseman, J. R.; Keith, T.; Petersson, G. A.; Montgomery, J. A.; Raghavachari, K.; Al-Laham, M. A.; Zakrzewski, V. G.; Ortiz, J. V.; Foresman, J. B.; Cioslowski, J.; Stefanov, B. B.; Nanayakkara, A.; Challacombe, M.; Peng, C. Y.; Ayala, P. Y.; Chen, W.; Wong, M. W.; Andres, J. L.; Replogle, E. S.; Gomperts, R.; Martin, R. L.; Fox, D. J.; Binkley, J. S.; Defrees, D. J.; Baker, J.; Stewart, J. P.; Head-Gordon, M.; Gonzalez, C.; Pople, J. A. *Gaussian 94*, Revision C.3; Gaussian, Inc.: Pittsburgh, PA, 1995.